Порфирины
Porphyrins

Макрогетероциклы
http://macroheterocycles.isuct.ru

Миниобзор
Microreview

Ligand Exchange Dynamics and Temperature Effects upon Formation of Nanocomposites Based on Semiconductor CdSe/ZnS Quantum Dots and Porphyrins: Ensemble and Single Object Measurements

Eduard I. Zenkevich,[a@] Thomas Blaudeck,[b] Danny Kowerko,[c] Alexander P. Stupak,[d] Frank Cichos,[e] and Christian von Borczyskowski[f]

[a]*National Technical University of Belarus, Department of Information Technologies and Robotics, 220013 Minsk, Belarus*
[b]*Linköping University, Department of Science and Technology, Organic Electronics, 60174 Norrköping, Sweden*
[c]*University of Zürich, Institute for Inorganic Chemistry, 8057 Zürich, Switzerland*
[d]*B.I. Stepanov Institute of Physics, National Academy of Science of Belarus, 220072 Minsk, Belarus*
[e]*Leipzig University, Institute of Experimental Physics I, Molecular Nanophotonics, 04103 Leipzig, Germany*
[f]*Institute of Physics and Center for Nanostructured Materials and Analytics (nanoMA), Chemnitz University of Technology, 09107 Chemnitz, Germany*
[@]*Corresponding author E-mail:zenkev@tut.by*

Dye molecules with pyridyl side substituents (porphyrins and heterocyclic perylene diimides) coordinatively attached to semiconductor CdSe/ZnS quantum dots (QDs) surface form quasi-stable "QD-Dye" nanocomposites of various geometry in the competition with capping molecules (tri-n-octyl phosphine oxide or long chain amines) exchange. This results in photoluminescence (PL) quenching of the QDs both due to Foerster resonance energy transfer and formation of non-radiative surface states. QD surface is inhomogeneous with respect to the involved attachment and detachment processes. The formation of "QD-Porphyrin" nanocomposites is realized at least two time scales (60 and 600 s), which is attributed to a reorganisation of tri-n-octylphosphine oxide capping shell. In a low temperature range of 220÷240 K related changes in QD absorption and emission reveal a phase transition of the capping shell (tri-n-octyl phosphine oxide and amine). In "QD-Dye" nanocomposites, this phase transition is enhanced considerably by only a few attached dye molecules and has impact on the QD core structure followed by changes of PL quenching and exciton-phonon coupling. A combination of ensemble and single molecule spectroscopy of "QD-Dye" nanocomposites reveals that few or even only one attached dye molecule change the surface distribution and energy of dye related surface trap states considerably.

Keywords: Semiconductor quantum dots, porphyrins, self-assembly, ligand dynamics, photoluminescence quenching, surface traps, fluorescence resonant energy transfer, temperature surface "phase" transition, single objects spectroscopy.

Introduction

At the moment, it is well-documented that *photonics* plays a pivotal role in advancing Nano/Bio/Info technology by creating new interfaces between multiple disciplines. In this respect, *nanophotonics* provides opportunities for high-density integration in information technology and for efficient harvesting of solar energy, while *nanobiophotonics* offers exciting opportunities for fundamental research to probe intercellular interactions as well as to produce novel nanoprobes for biomedical imaging, biosensing and therapy for cancer as well for other major medical needs to advance human health. In this respect, nanostructured materials with tuneable morphology have attracted exceptional interest over the past decades because of their unique architectures, tailored physicochemical properties, central roles in fabricating nanoelectronics, and potential applications in bionanotechnology.[1-8]

Recently, great efforts have been devoted to bottom-up self-assembled nanostructures. Self-assembly is the fundamental phenomenon that generates structural organization on all scales *in vivo* and *in vitro*.[9] The most important source of inspiration for self-assembly strategies is natural photosynthesis in which the generation of complex, multicomponent three-dimensional structures involves intramolecular, as well as intermolecular and interfacial interactions.[10,11] In the organic world, the preparation of supramolecular architectures in which organic compounds present a high degree of order, which spans from the nanoscopic to the macroscopic level across multiple length scales, is highly desirable and represents a key issue within the fast-growing fields of nanoscience and nanotechnology.[12-20] In this respect, the interest in emerging organic nanostructures formed via the bottom-up approach (including those based on tetrapyrrolic macrocycles) is growing exponentially since they are not only good models for mimicking the primary

photochemical processes *in vivo* but seem to be considered as promising building blocks for advanced multifunctional nanocomposites with potential applications in improved drug delivery systems, photodynamic therapy, nanovoltaic cells, optoelectronic memory, multimolecular architectures for information storage and highly efficient catalysts.[21-26] However, many fundamental issues still need to be in-depth investigated in order to have full understanding of mechanisms that drive the properties of organic nanocomposites.

The field of nanoscience and nanotechnology is extending also the applications of physics, chemistry, engineering and technology into inorganic systems of nanoscale dimensions. In this connection, semiconductor nanocrystals (often referred to as quantum dots, QD, *e.g.* CdSe or CdSe/ZnS and other II-VI systems) represent a specific class of matter between atomic clusters and bulk materials with well-defined size-dependent tunable photophysical properties.[27-30] Correspondingly, based on ideas of the self-assembly discussed above, *the combination of the two directions*, that is the anchoring of functional organic molecules (including tetrapyrrolic compounds and other heteromacrocycles) or molecular complexes or even proteins to QDs, is of considerable scientific and a wide practical interest including material science and biomedical applications.[31-38]

Inspired by our earlier work on self-assembled multiporphyrin arrays[39-45] we have elaborated the experimental approach in the direct labelling of trioctylphosphine oxide (TOPO)- and amino (AM) -capped semiconductor quantum dots (QD) CdSe/ZnS with functional ligands (dyes) of two types (pyridyl substituted porphyrins and heterocyclic pyridyl functionalized perylene diimide molecules) in liquid solutions and polymeric matrixes.[46-55] We have shown that depending on redox and electronic properties of interacting subunits as well as anchoring groups (connecting organic and inorganic counterparts) the formation of "QD-Dye" nano-composites allows for a controlled realization of mutually relative (spatial) orientations and electronic energy scales in order to optimize intended photoinduced processes such as charge transfer,[56,57] fluorescence Foerster energy transfer (FRET)[20,46,47,50,52] or electron tunnelling in the conditions of quantum confinement (non-FRET process).[48,50,53] Typically, all these processes lead to the pronounced quenching of QD photoluminescence (PL) in nanocomposites that may be used as an indicator of complex interface phenomena selectively depending on attached ligands (porphyrins, perylene diimides, *etc.*).

It should be mentioned that self-assembled "QD-Dye" nanocomposites present a quintessential problem for surface and interface science. Correspondingly, with respect to formation and possible applications of these nanocomposites in the liquid or solid phase (*e.g.* in sensing phenomena[37,58] or photodynamic therapy[53,59-61]) several factors related to the QD PL efficiency are of essential importance: (i) attachment/detachment of heterocyclic dye molecules,[46,62-65] (ii) the interplay of dye molecule attachment and ligand exchange dynamics[66,67] and (iii) the presence and formation of various surface trap states in the band gap,[68,69] whose energies and corresponding quenching efficiencies may be changed upon interface reconstruction (via polarity and/or temperature change) or competing ligand/dye exchange dynamics.

The intention of this semi-review paper is not a thorough description of all the relaxation processes in "QD-Dye" nanocomposites, which would be too early given some open problems as well as some specific structural aspects. Rather the present work should be viewed as a more comparative characterization of the non-covalent self-assembly possibilities and the dynamics in these systems, thus providing the data for a further development of defined multicomponent structures for exploitation as artificial light-harvesting complexes, electro- and photochemical devices, nanosensors, *etc*. There are several objectives of this report. One goal is to familiarize the reader with a specific role of porphyrin *meso*-phenyl substituents in the nanocomposite formation and exciton relaxation dynamics. Then we are willing to demonstrate that the QD surface is inhomogeneous with respect to the involved attachment and detachment processes, *i.e.* the formation of "QD-Dye" nanocomposites is in competition with TOPO and AM capping molecules exchange dynamics. Finally, we plan describe that very few or even only one attached porphyrin molecule change the distribution and/or presence of dye related surface trap states considerably, and the "decoration" of QDs by dye molecules makes a phase transition of the QD capping ligand shell (at low temperatures) highly visible or even amplifies the phase transition. Notably, in order to obtain more insight about these processes we used a combination of bulk and single molecule/single quantum dot experiments as a tool to precisely identify the interaction of exactly one QD with one dye molecule leading to a microscopic understanding of the "QD-Dye" nanocomposites formation (including ligand dynamics) and related mechanisms of PL quenching dynamics. On the basis of these well-documented understandings, one could search functional nanocomposites for possible application in various fields of nanoscience and nanotechnology.

Experimental

Colloidal Semiconductor CdSe/ZnS Quantum Dots

For ensemble and single particle experiments colloidal core/shell CdSe/ZnS QDs passivated by tri-*n*-octyl phosphine oxide (TOPO) or long-chain amines (AM) were obtained from Evident Technologies, Inc, Troy, NY, USA. The absorbance of the QD starting toluene solution was adjusted to be lower than 0.1 OD at excitation and emission wavelengths in order to avoid non-linear absorption and re-absorption effects. The concentrations varied in the range $(1 \div 10) \cdot 10^{-7}$ M. In ensemble experiments stability and purity of the QD solutions were checked by measuring the quantum yield stability at least over 3 hrs after preparation. The properties of the used QDs are presented in our earlier papers.[46,48,52,54]

Pyridyl Functionalized Dye Molecules

Like in the case of multiporphyrin complexes,[15,18,20,39,40] the selective replacement of *meso*-phenyl rings in tetra-phenyl porphyrins by pyridyl rings, $H_2P(Pyr)_n$ as well as $CuP(Pyr)_4$, offers the possibility for a controllable formation of "QD-Porphyrin" nanocomposites via a coordination "key-hole" principle.[20,46,48,49] It is well-known from chemical background that the 3*d* transition metal Zn^{2+} ion has empty $3d^{10}$ orbital while heteroatom N-pyr of the porphyrin *meso*-pyridyl ring is a very good e-donor having an unshared electron pair. Correspondingly, in this case a "key-hole"

principle is realized via one- or two-fold non-covalent coordination Zn····N(pyr). Synthesis and spectral details of *meso*-pyridyl containing porphyrins have been reported earlier.[39,40] In ensemble experiments, porphyrin stock solutions were prepared in toluene under ultrasonic treatment at 40°C at concentrations in the range $(3 \div 30) \cdot 10^{-5}$ M.

For single particle experiments, sufficiently high photostable pyridyl functionalized perylene diimide molecules were used. The synthesis of these compounds is described elsewhere.[70,71] In the present experiments we have used (pyridyl)₁-perylene diimide (PP).

Sample Preparation

Quantiative titration experiments have been performed in case of ensembles at ambient conditions with toluene spectroscopic grade (Fluka SeccoSolv or Merck dried with a molecular sieve). The optical cuvettes (Hellma QS-111, path length 1 cm) and other glassware were flushed with acetone and ethanol, chemically cleaned with aqueous H_2SO_4:H_2O_2, flushed with deionized water, dried in a nitrogen flow and purged with toluene. Temperature $(77 \div 300$ K) measurements for QDs and "QD-Porphyrin" nanocomposites were carried out in a methylcyclohexane/toluene (6:1) mixture possessing an optical transparent glass at low temperatures. The respective glass transition temperatures are the following:[72] 146.7 K (methylcyclohexane), 180 K (toluene), and 151.6 K (methylcyclohexane/toluene 6:1 mixture). For single particle experiments samples, pipettes and vials were thoroughly cleaned by supersonic treatment in a piranha solution (1:1 H_2O_2-H_2SO_4 solution) and by careful rinsing with Millipore DI water. Material quality was checked with a homebuilt fluorescence wide field microscope. Initial stock QD-dye solutions at a given molar ratio have been prepared by one step mixing at concentrations in the range of $10^{-6} \div 10^{-7}$ M. Then for single nanoobjects experiments, these solutions have been additionally diluted, and single particle sample preparation was done by spin coating a $\sim (1 \div 5) \cdot 10^{-11}$ M

solution of the QD-dye mixture onto a Si/SiO₂ (100 nm thick SiO₂) surface. Structures of 5,10,15,20-*meso*-metapyridyl substituted porphyrin (H₂P) and (pyridyl)₁-perylene diimide (PP) molecules, capping molecules of tri-*n*-octyl phosphine oxide (TOPO) and long-chain amines (AM) are depicted in Figure 1. Figure shows also a schematic representation (not on scale) of "QD-porphyrin" (A) and "QD-perylene diimide" (B) nanoassemblies and mutual arrangement of dye molecules with respect to QD surface.

Experimental Techniques

In ensemble experiments, absorption spectra were recorded with a Shimadzu 3001 UV/Vis or Cary-500 M Varian spectrometer. Emission spectra were measured with a SFL-1211A (Solar, Belarus) or Shimadzu RF-5001PC spectrofluorimeter. Temperature experiments were carried out using a home built cryostat (Solar, Belarus) equipped with a temperature controller (ΔT=0.5 K). QD and dye emission decays (time correlated single photon counting mode, TCSPC) were measured using a laboratory spectrofluorometer equipped with computer module TCC900 (Edinburg Instruments) and light emitting diodes (PicoQuant GmbH): PLS-8-2-130 (λ_{max}=457 nm, FWHM~ 713 ps) and PLS-8-2-135 (λ_{max} =409 nm, FWHM~990 ps).

At ambient conditions, single particle experiments (PL spectra and decays) were performed in a home built laser scanning confocal microscope[51,52,54] depicted schematically in Figure 2. Shortly, the main features of this experimental setup are as follows. A Peltier-cooled pulsed laser diode ("LDH-P-C 470", Picoquant) emitting pulses of 75 ps length at λ= 465 nm (tunable repetition rate of 1/32÷80 MHz) was used in this setup. The samples were mount on a close-looped piezo 3D-translation stage (Piezosystems, Karl Zeiss, Jena) with a maximum scan range of 80 μ. The emitted light is separated by a neutral beam splitter (3:1) and focused by the final achromatic lens to the entrance slit of a spectrometer and a single photon counting avalanche photodiode (APD). The excitation pulse width allows a TCSPC time resolution down to 75 ps, the time jitter
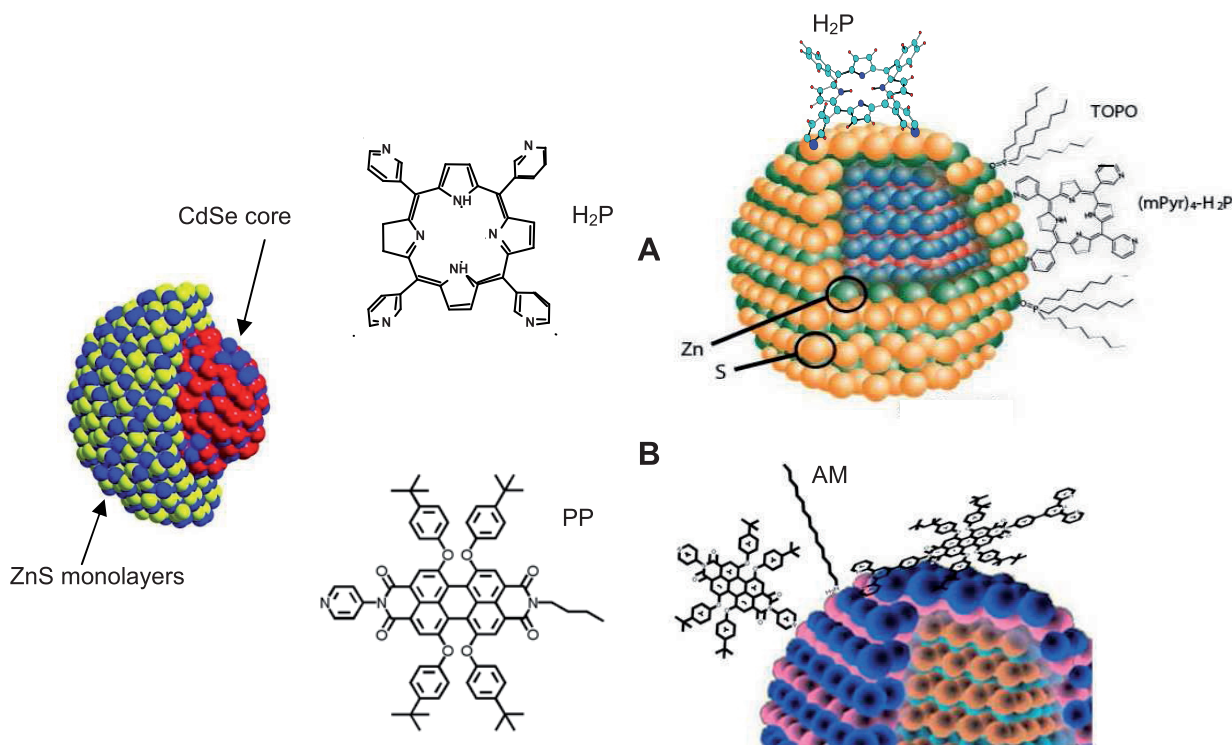

Figure 1. Schematic structural presentation of "QD-porphyrin" (A) and "QD-perylene diimide" (B) nanocomposites with corresponding displacement of dye molecules with respect to the QD surface for (A) and (B) nanoassemblies. Main structural features for 5,10,15,20-*meso*-metapyridyl porphyrin H₂P(Pyr)₄ and (pyridyl)₁-perylene diimide (PP) molecules as well as for capping ligands, tri-*n*-octyl phosphine oxide (TOPO) and long-chain amines (AM), are presented also.
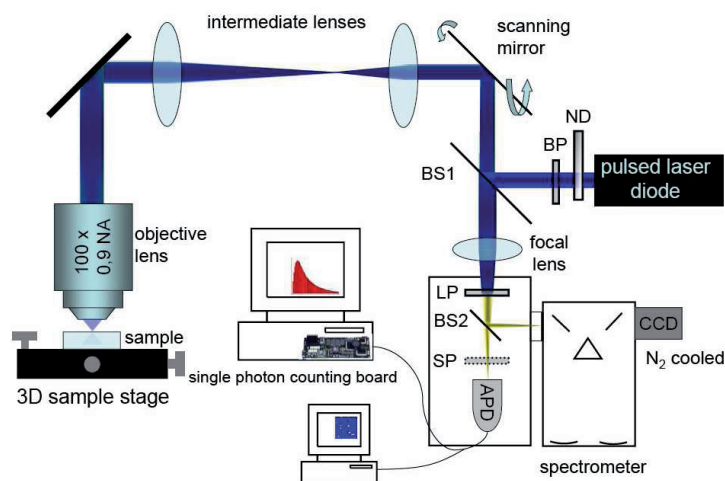
Figure 2. Scheme of the confocal microscope setup applied for single molecule, quantum dot and nanocomposite spectroscopy. Abbreviations: ND - neutral density filter, BP - band pass filter, BS - (neutral) beam splitter, LP - long pass filter, SP - short pass filter.

of the APD downgrades this value to about 700 ps. Emission decays have been measured in time-tagged time-correlated single photon counting (tt-TCSPC) mode permitting generation of PL intensity and PL lifetime time traces with any desired binning time after the experiment. Autocorrelation functions and inter-photon duration statistics derived from tt-TCSPC data provide insight into blinking dynamics of single emitters. Spectra were recorded with a highly sensitive spectrometer ("Acton SpectrPro-275", Acton Research Corp.) equipped with a liquid nitrogen cooled CCD detector. Sequences of single emitter spectra are typically recorded with a time resolution in the range of seconds to several hundreds of milliseconds.

Results and Discussion

Comparative Titration Experiments and Nanocomposite Formation

Typically, at ambient temperature, the titration of CdSe/ZnS QD toluene solution by a comparable amount of *meso*-pyridyl substituted porphyrins $H_2P(Pyr)_n$ results in the QD photoluminescence (PL) quenching (emission intensity decrease and decay shortening,[46,48-50] Figure 3). These results clearly indicate the formation of "QD-Porphyrin" nanocomposites via anchoring *meso*-pyridyl rings with ZnS surface of QD.

Stimulated by experience with self-assembled porphyrin arrays we have systematically studied the specificity of QD-porphyrin interactions upon exchange competition with TOPO capping molecules. The strategy was to carry out titration experiments for QD with fixed parameters (size and number of ZnS monolayers) but using *meso*-pyridyl substituted porphyrins $H_2P(Pyr)_n$ with changed properties such as: (i) the number of pyridyl-rings from 1 to 4 including the two variants for the displacement $(m-Pyr)_2$- and $(m^\wedge Pyr)_2$-, where pyridyl rings are opposite or adjacent to each other; (ii) for the four-fold pyridyl substituted H_2P the type of N-substitution within the pyridyl ring from *meta*- (*m*) to *ortho*- (*o*) and *para*- (*p*) N position (Figure 4A).

It is seen from Figure 4B that $H_2P(o-Pyr)_4$ and $H_2P(m-Pyr)_2$ porphyrins almost do not quench the QD PL (curves 1,

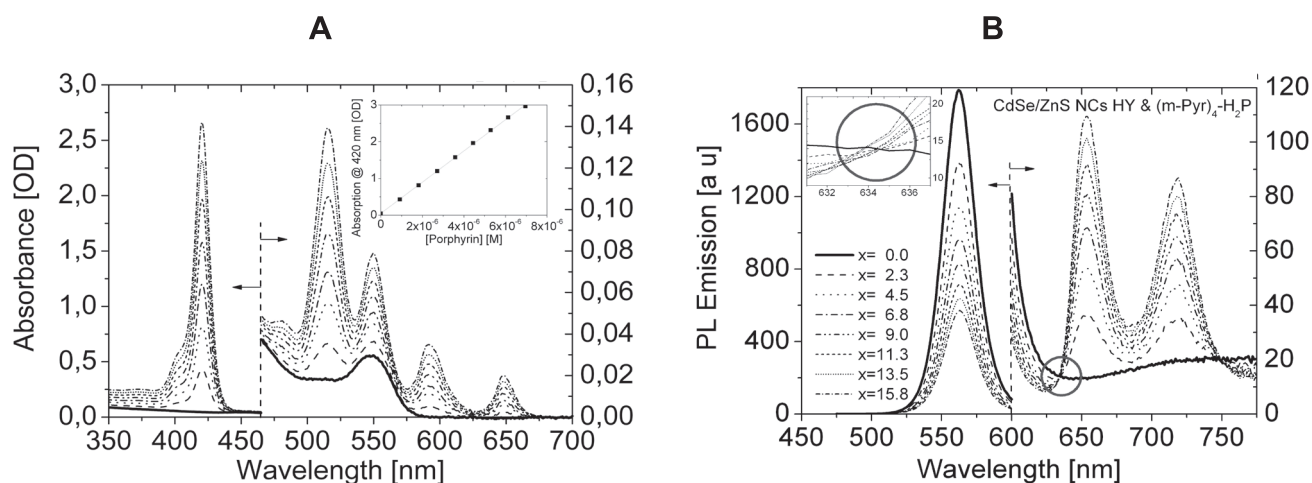**Figure 3**. Absorption (A) and emission (B, λ_{ex} = 465 nm) spectra of CdSe/ZnS QD (d_{CdSe} =3.0 nm, 2 ZnS monolayers, C_{QD} = 4·10^{-7} M) and $H_2P(m-Pyr)_4$ molecules upon molar ratio *x* increase. Inset in A: peak intensity of the Soret band as function of the nominal concentration. Deviations from linearity represent the uncertainty in the amount of added substance (*i.e.* 5.0 ± 2.5 %). Circle in B shows the existence of quasi-isosbestic point in emission spectra upon titration.
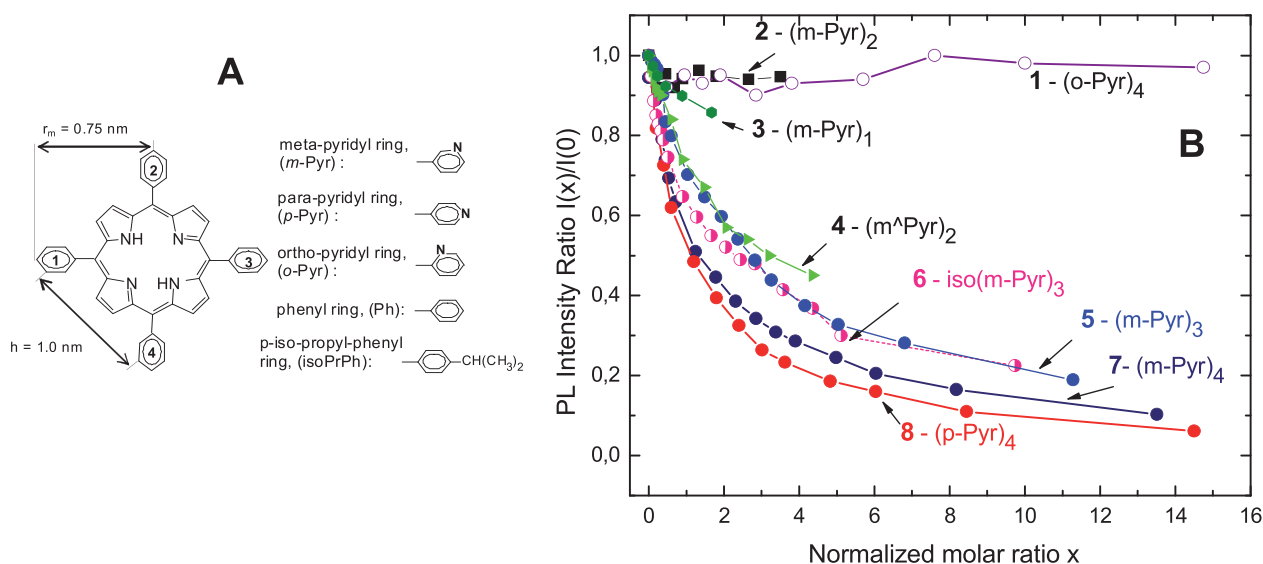
Figure 4. *A*: Chemical structure, abbreviation and positions of *meso*-substituents for porphyrin molecules. $r_m = 7.5$ Å is the radius of porphyrin molecule with opposite pyridyl rings having nitrogens in *meta*-positions, h = 10 Å is the mean distance between *meta*-nitrogens of adjacent pyridyl rings (HyperChem software, release 4.0 geometry optimization with semiempirical PM3 method). *B: Relative photoluminescence intensity dependence* $E = I(x)/I(0)$ for CdSe/ZnS QD (d_{CdSe} =2.5 nm, 2 ZnS monolayers, $C_{QD} = 4 \cdot 10^{-7}$ M) on the molar ratio ($x = [C_{porph}]/[C_{QD}]$) for various porphyrin molecules: 1 - $H_2P(o\text{-Pyr})_4$; 2 - H_2P $(m\text{-Pyr})_2(Ph)_2$; 3 - $H_2P(m\text{-Pyr})_1$; 4 - $H_2P(m^\wedge Pyr)_2$; 5 - $H_2P(m\text{-Pyr})_3$; 6 - $H_2P(iso)\text{-}(m\text{-Pyr})_3$; 7 - $H_2P(m\text{-Pyr})_4$; 8 - $H_2P(p\text{-Pyr})_4$.

2), whereas the quenching is strongest for $H_2P(p\text{-Pyr})_4$ and $H_2P(m\text{-Pyr})_4$ ones. Within the $H_2P(m\text{-Pyr})_4$ manifold, there is a systematic increase of the quenching efficiency on the number (*n*) of *meso*-pyridyl substituents. From the absence of QD PL quenching in the case of $H_2P(o\text{-Pyr})_4$ and $H_2P(m\text{-Pyr})_2$ porphyrins, we conclude that despite the flexibility of pyridyl rings with respect to the H_2P macrocycle, a parallel orientation of the macrocycle with respect to the QD surface is obviously not favoured. However, an orientation of the porphyrin macrocycle nearly perpendicular to the QD surface would be easily possible for *meta* and *para* N positions in pyridyl substituted porphyrins (see Figure 1A). Like for porphyrin self-assembled triads,[40] the importance of the designed two-point interacting domain is also demonstrated upon formation of "QD-Porphyrin" nanocomposites. This process is based essentially on a "Lego-type" key-hole principle effectively controllable via steric factors, distance matching, optimization of relative orientations, and solvent composition.[46] It is also clear that the attachment of porphyrin molecules to QD surface is realized in the competition with capping TOPO molecules. Notably, in contrast to toluene, the PL intensity of the QDs does not change in *n*-octane indicating that the capping TOPO shell is stabilized against the H_2P molecules in the later case.

When numerically analysing QD PL quenching data for various porphyrin molecules in order to evaluate of the corresponding complexation constants K_C one should take into account few aspects: ligands exchange dynamics (depending on TOPO concentration and solvent properties) and number of H_2P molecules per QD. Without consideration of the dynamic equilibrium, it is reasonable to assume that the PL quenching rate for a given QD with n attached chromophores is proportional to n, whatever the quenching mechanism is (in our case, due to both FRET and electron tunnelling in the conditions of quantum confinement[46,48,49]).

Like it has been done earlier[73] as well as in our publication[46] and in recent publications,[74,75] QD-porphyrin interaction may be described by a Poisson distribution:

$$P(n) = x^n \exp(-x)/n! \qquad (1),$$

where *x* is the average number of chromophores per one QD (estimated from a molar ratio ($x = [C_{porphyrin}]/[C_{QD}]$), *n* is the number of attached chromophores on a given QD. Correspondingly, the QD PL intensity ratio $I(x)/I_0$ may be written as

$$I(x)/I_0 = e^{-x}\Sigma x^n/n!(1+nk_Q/k_D)^{[73]}$$

or

$$\frac{I(x)}{I_o} = \sum_{n=o}^{\infty} \frac{k_D}{k_D + nk_Q} x^n \frac{\exp(-x)}{n!} \quad ^{[76]} \qquad (2),$$

where k_D is the total QD PL intrinsic decay rate and k_Q the QD PL quenching rate. Using this approach, it was found that the estimated values of complexation constant K_C for "QD-Porphyrin" nanocomposites lie in the region from ~10^5 M^{-1} (for $H_2P(m\text{-Pyr})_1$) to ~10^7 M^{-1} (for $H_2P(m\text{-Pyr})_4$).[50,55,76] The details of this approach including also the analysis of time resolved kinetics of QD PL decays will be presented in the forthcoming paper.

Manifestation of Temporal Porphyrin and Capping Ligand Exchange Dynamics

A comprehensive description of capping molecules and porphyrin ligands dynamics in relation to PL quenching processes is of crucial importance for the elucidation of

mechanisms of photoinduced processes in "QD-Porphyrin" nanocomposites (as well as for other dyes) as a step to an investigation of the chemical topography of QD surface. Here, we focus presumably on nanocomposites based on TOPO-capped CdSe/ZnS QDs and $H_2P(m\text{-Pyr})_4$ molecules (or H_2P, Figure 1A) showing among a series of pyridyl substituted free-base porphyrins the most effective PL quenching of QDs at the same titration conditions (Figure 4B). Due to the simultaneous observation of FRET and non-FRET PL quenching processes for QDs in "QD-Porphyrin" nanocomposites,[46-50,53] which serves as an indicator for the nanocomposite formation we have the direct access to QD surface-related processes. The detailed analysis of a whole series of titration experiments to study the PL intensity of CdSe/ZnS QDs as a function of the added amount of $H_2P(m\text{-Pyr})_4$ molecules within time scale from 60 s to minutes and hours as well as of solvent (toluene or *n*-octane) has been presented in our recent paper.[54] Here, we would like to pick out main results (marked below by bold numbers) and conclusions.

(1) Addition of the porphyrin aliquot to the master solution of QDs (with or without ZnS) results in an immediate decrease of the PL intensity faster than our time resolution of about 60 s. In each of the samples, the initial fast PL decrease is followed by a decrease of the PL intensities on longer time scales (Figure 5A,B). The PL decrease decay seems to be broadly distributed reflecting the presence of different quenching processes, namely those already inherent in the pure QD sample and those imposed by addition of the H_2P resulting in assembly formation.

(2) FRET efficiency increases on a time scale of minutes before it either saturates in a constant value for some more minutes (nicely seen for [QD]=$1\cdot10^{-7}$ M Figure 5B) or proceeds already with a slight decrease within longer time scale. In this case, FRET is a measure for the formation kinetics of "QD-Porphyrin" nanocomposites.

(3) QD PL quenching upon titration by porphyrins scales inversely with QD concentration. The decrease for later times is an obvious result of the ongoing (independent of porphyrin) intrinsic PL quenching for QD (Figure 5A) which reflects the particular dynamic processes at the QD surface and has a direct feedback on the FRET efficiency. The comparison of the PL quenching with the FRET build-up during time shows that the "QD-Porphyrin" nanocomposite formation has multiple (at least three) macroscopic time scales.

For the analysis of the PL quenching as a function of the number of H_2P molecules per QD, the well-known Stern-Volmer formalism[77] was appropriately modified,[48] and this quenching can be described by

$$\frac{I_0}{I(x)} = 1 + \int_0^\infty K(x)\cdot dx \,.$$ (3)

In this approach, the Stern-Volmer function $K(x)$ depends explicitly on the molar ratio $x = [C_{porph}]/[C_{QD}])$ and is expressed as the first derivative of the experimental data plotted in Stern-Volmer representation. Further, the evaluated from titration curves $K(x)$ values can be written as

$$K(x) = k_q(x)\cdot\tau_0$$ (4),

where k_q corresponds to the total quenching rate induced by the number of quencher molecules actually present (depending on the molar ratio x) and τ_0 to the intrinsic PL lifetime of the QD in absence of quencher molecules. The results based on the analysis of the Stern-Volmer plots, are as follows (Figure 6).

(4) Figure 6A reveals the linear relationship between the quenching constant $K(x=1)$ (determined for small molar ratios) and the reciprocal absolute concentration
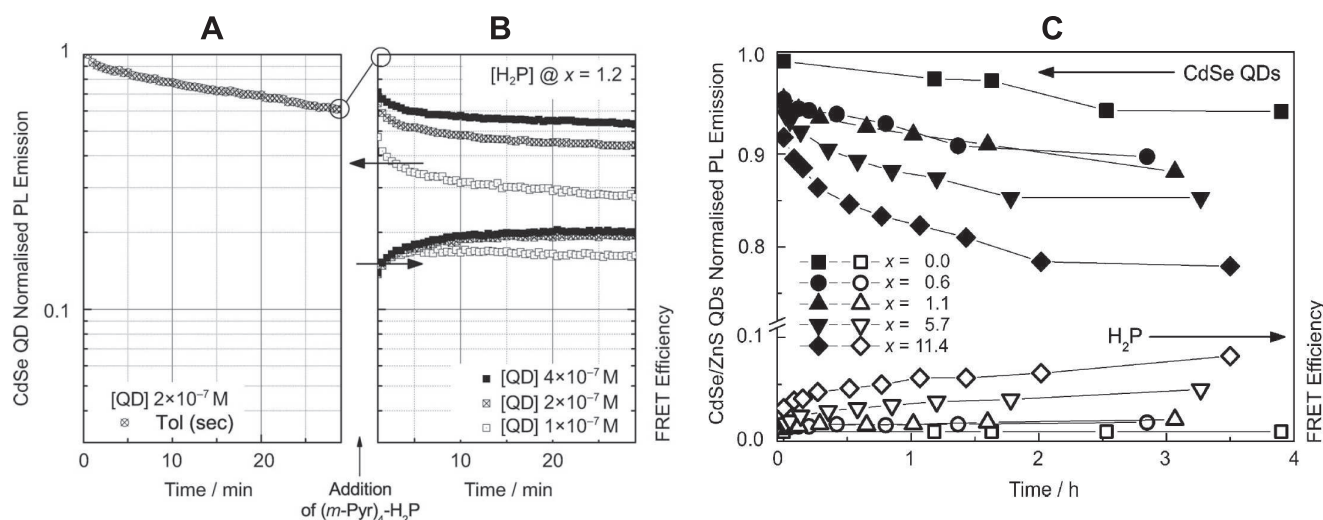

Figure 5. Influence of sample conditions on the time dependent QD PL quenching and FRET efficiency (relative units) for "QD-Porphyrin" nanocomposites based on QDs and $H_2P(m\text{-Pyr})_4$ molecules in toluene at 293 K. For all dependences, left scale is QD normalized PL emission, right scale is experimental FRET efficiency QD→porphyrin calculated according to the procedure described in our previous papers.[46,48,53] *A:* Time dependent emission for alone CdSe QD (d_{CdSe} =3.0 nm, [C_{QD}]=$2\cdot10^{-7}$ M). *B:* Time dependent emission for CdSe QD (d_{CdSe} =3.0 nm) and FRET efficiencies for nanocomposites at constant molar ratio x = 1.2 for three initial QD concentrations. *C:* Long-time development of the PL of CdSe/ZnS QDs (d_{CdSe}= 3.0 nm, 2 ZnS monolayers) and FRET efficiency for "QD-Porphyrin" nanocomposites at different molar ratios.

[QD]$^{-1}$, respectively. The linear dependence indicates that the underlying quenching processes have a common nature for all absolute initial concentrations of QDs. The observed linearity is changed upon molar ratio increase. This indicates that, when deviating from the low-concentration regime, additional dynamic constraints such as ligand dynamics to create new attachment sites which control the QD PL aside of the immediate assembly formation.

(**5**) Titration experiments with QDs of a variable size (Figure 6B) show also that $K(x)$ is indeed initially constant but becomes smaller around a critical molar ratio (which we will call $x_c \approx 1 \div 10$ depending on QD size). This critical molar ratio x_c increases more or less systematically with the diameter of the QD.

(**6**) Finally, it follows from ensemble and single object experiments for "QD-perylene-diimides" nano-composites,[51,52] that the number of attached dye molecules to a QD is much less than that given by the molar ratio x. We assume that a similar situation holds also for H$_2$P just after titration step. Indeed, QD PL quenching is still increasing in the presence of H$_2$P while also FRET increases at long waiting times (see Figure 5C) up to > 24 h.[51,52] It means that at very high H$_2$P concentrations and long waiting times the TOPO capping shell becomes nearly completely replaced by H$_2$P molecules.

The overall interpretation of the above findings is that because of the presence of a limited number of empty attachment sites on the QD surface, QD PL quenching in "QD-Porphyrin" nanocomposites occurs in two steps. (i) Immediately after titration, nanocomposites are effectively formed, which results in both QD PL quenching and FRET QD→H$_2$P.[46] (ii) More porphyrin molecules become attached during the waiting time. However, increased QD PL quenching and FRET are not exactly on the same quantitative level. Clearly the titration step also favors other competitive quenching mechanism (electron tunneling in the conditions of quantum confinement[48]) in addition to FRET. It means that the exciton relaxation dynamics in QD

initiated by a single titration step is not only due to the added H$_2$P molecules themselves, but also to a local change in the capping ligand shell on QD surface upon nanocomposite formation as well as to a local replacement of TOPO by H$_2$P molecules as suggested earlier.[78,79] This argumentation is in line with the finding that dilution of a QD solution reduces the average coverage of the QDs with TOPO,[51,52] giving rise to both an intrinsic reduction of QD PL[80] as well as to increased accessibility of the QD surface to the quencher molecules. It should be mentioned also that the capping ligand coverage (TOPO or amines), and thus, the number of accessible attachment sites are controlled by the solvent polarity. Since these processes may depend on several partly hidden conditions, such as QD surface structure and absolute TOPO concentration, they vary from sample to sample and QD to QD. However, though absolute values differ from each other considerably, we observed the same qualitative behavior in all cases.

Recently, based on these ideas, we have carried out a quantitative experimental analysis (steady-state and picosecond time-resolved measurements) of QD photoluminescence quenching in nanocomposites based on TOPO capped CdSe/ZnS QDs (d_{CdSe} = 3.0 nm, 2 ZnS monolayers) and H$_2$P(m-Pyr)$_4$ molecules at molar ratio $x = 4$ in toluene at 295 K.[53] Our results have shown that in these nanocomposites, the main part of quenching is due to non-FRET process (the electron tunneling with the efficiency of $\Phi_{non-FRET}$ = 0.85÷0.90), while FRET QD→porphyrin occurs with quantum efficiency of Φ_{FRET} = 0.10÷0.15. In addition, using near-IR photoluminescence measurements, we performed a comparative studying the efficiencies of the singlet oxygen ($^1O_2$) generation by alone QDs and "CdSe/ZnS QD-Porphyrin" nanocomposites. It was found that in the later case the experimental efficiencies γ_Δ of $^1O_2$ generation are essentially higher with respect to those obtained for alone QDs. It has been found also that within the accuracy of the experiment for these nanocomposites, that the values of FRET efficiencies obtained via the direct $^1O_2$ emission
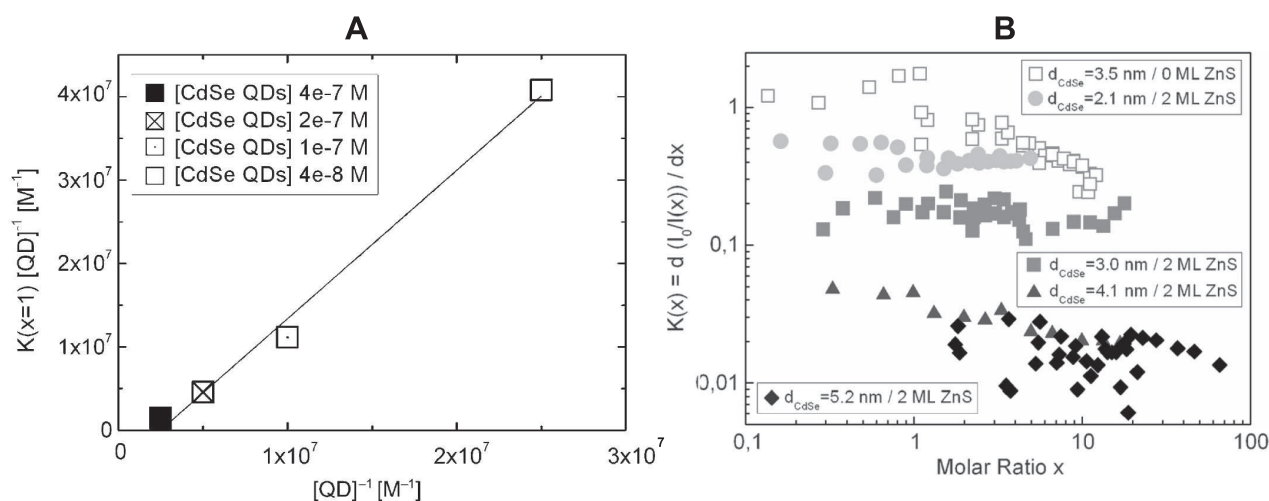

Figure 6. Dependence of QD PL quenching (Stern-Volmer values $K(x)$ evaluated according to Equation 3) on QD initial concentration [C_{QD}] (A) and QD size (B) for "QD-Porphyrin" nanocomposites in toluene at 293 K.[54] *A*: The slope $K(x=1)$ (low-molar-ratio regime at constant molar ratio) upon the QD initial concentration [C_{QD}] increase. *B*: PL quenching as a function of the molar ratio x for QDs of various sizes and types (without and with 2 ZnS monolayers, ML) at fixed QD initial concentration [C_{QD}]=1·10^{-7} M). The double logarithmic plot shows the clear dependence of the PL quenching on the QD size.
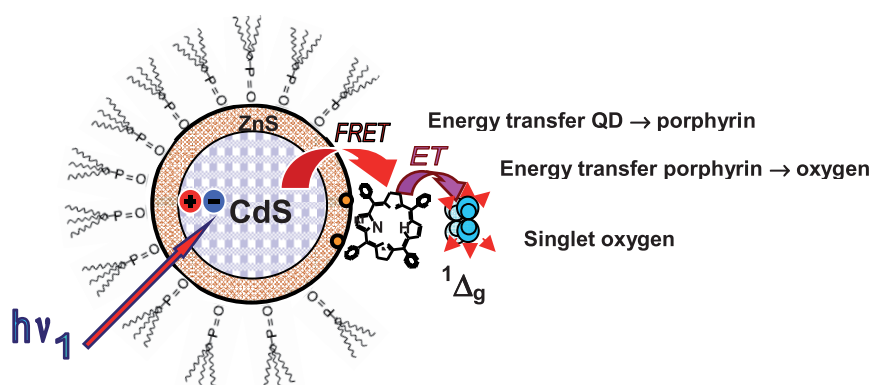
Scheme 1.

measurements at low laser excitation ($\Phi^{\Delta}_{FRET} = 0.12 \pm 0.03$), are in a good agreement with FRET efficiencies found from the direct sensitization data for porphyrin fluorescence ($\Phi_{FRET} = 0.14 \pm 0.02$). Such quantitative analysis was done for the first time and shows that namely FRET process QD→porphyrin is a reason of singlet oxygen generation in the given nanocomposites according to the following scheme:

The obtained results may be considered as a direct proof of the realization of namely FRET QD→porphyrin process followed by the singlet oxygen generation via porphyrin triplet states. All these facts raise the hypothesis that "CdSe/ZnS QD-porphyrin" bioconjugates have a potential to be photosensitizers of a novel type in the photodynamic therapy of cancer.

Ligand Capping Phase Transitions in "QD-Dye" Nanocomposites upon Temperature Lowering

In the following two sections, we discuss the influence of structural surface transformations such as a capping layer (TOPO or AM) temperature induced phase transition and QD photodegradiation on the optical properties of QDs, especially how they are related to the nanocomposite self-assembly and connected with PL quenching and exciton-phonon coupling in QDs. Our comparative results are concerned with (77÷300 K) temperature dependent optical

properties of "QD-porphyrin" nanocomposites (ensemble experiments) as well as on long-term temporal evolution of PL spectra (photodegradition related to interface transformation processes) for QDs assembled with perylene diimides (ensemble and single particle detection). In case of porphyrin we report on the (temperature dependent) formation of CdSe/ZnS trap states in competition to QD near band edge (excitonic) states. While the detailed results of all series of experiments are still under investigation and will be discussed in a forthcoming paper, we will concentrate here on the temperature dependent influence of dye (presumably porphyrin) molecules on the QD PL and will only present those results on ensembles of QDs, which are necessary to follow the overall behavior. The temporal variation of trap and near band edge states have been studied with a diimide dye using ensemble and single object detection. We will show that the combination of bulk and single molecule/single particle experiments[51,52,55] is a tool to precisely identify the interaction of exactly one QD with one dye molecule leading to a microscopic understanding of the formation (including ligand dynamics) and related mechanisms of PL quenching dynamics for "QD-Dye" nanocomposite nanoassemblies.

A set of typical absorption spectra (in the energy range of the first excitonic transition) and PL spectra for alone CdSe/ZnS QDs (without porphyrins, $d_{CdSe} = 3.0$ nm, 2 ZnS monolayers) at various temperatures is depicted in Figure 7. It is seen that upon temperature lowering, the band-edge

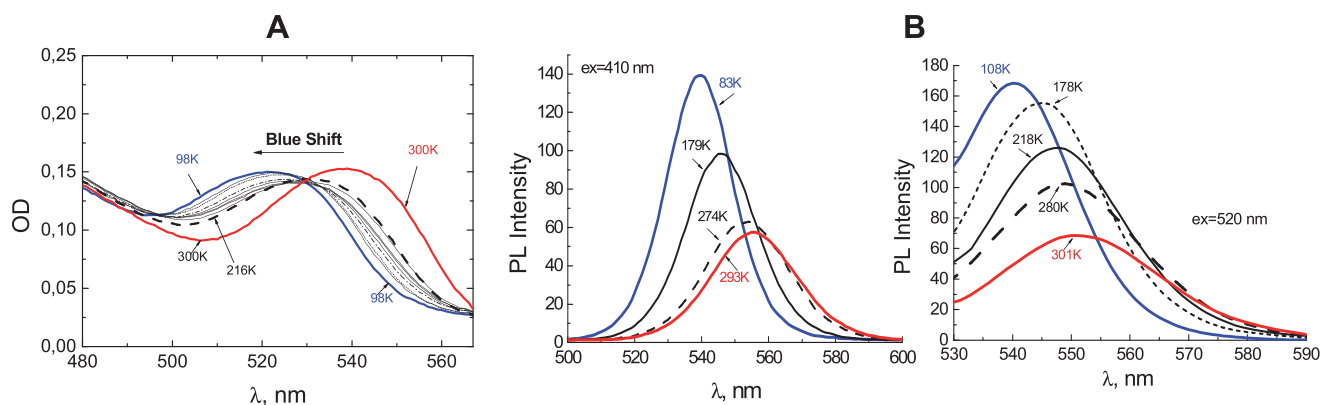**Figure 7**. Temperature dependence of absorption (*A*) and PL (*B*) spectra for CdSe/ZnS QDs without dyes ($d_{CdSe} = 3.0$ nm, 2 ZnS monolayers) in methylcyclohexane/toluene (6:1) mixture. Base line and straight light are subtracted in absorption spectra. PL spectra at various temperatures are presented for two excitation wavelengths.

absorption for alone QDs is blue shifting. The temperature dependence of the PL peak energy behaves similar as the band-edge absorption, that is manifests the blue upon temperature lowering. At 295 K excitation between 410 to 500 nm results in a PL band at λ_{max} = 555 nm, while upon excitation in the range of 510 ÷ 540 nm the PL band is characterized by λ_{max} = 551 nm. These results reveal that in addition to site selection (observed for QD PL[81]) the presence of at least two luminescent states is characteristic to QDs under study. Upon temperature lowering PL spectra are not only shifted to the blue, but also the line width (FWHM) becomes essentially narrower, while the PL intensity becomes higher. Based on considerations presented in our very recent paper[54] it may be concluded the QD PL quantum efficiency increases upon temperature lowering and PL emission takes place presumably from only one type of state.

Fitting the lowest absorption and PL bands position in the energy scale by a Gaussian components shows that besides the above mentioned blue shift upon temperature lowering a non-monotonous temperature dependence of the respective peak energies becomes evident (Figure 8).

It is seen in Figure 8A that non-monotonous behavior (which we name for simplicity "kink") is observed for TOPO-capped CdSe/ZnS QDs between 200 and 240 K, far from the glass transition temperatures for methylcyclohexane (146.7 K) and toluene (180 K), respectively as well as for a methylcyclohexane/toluene (6:1) mixture (151.6 K).[72] With T lowering the "kink" occurs at slightly different temperatures for the first excitonic absorption band (~218 K) and the PL band (~223 K), respectively. We also found, that a similar "kink" is observed in the PL temperature dependence for CdSe/ZnS QDs capped by long-chain amines (Figure 8B). In the later case, the "kink" in PL spectra is more pronounced and shifted to ~237 K as compared to ~223 K for TOPO-capped CdSe/ZnS QDs. Notably, this non-monotonous behavior becomes stronger for amine-capped CdSe/ZnS QDs with attached DPP dye molecules at molar ratio $x = [C_{DPP}]/[C_{QD}] = 1$, while no "kink" is observed when following the

luminescence of perylene diimide or porphyrin molecules under the same conditions (will be presented and discussed below). From these observations, we therefore exclude, that the morphology of the matrix is changing.

Typically, the PL blue shift and intensity rise upon temperature lowering is a commonly observed phenomenon for QDs and is generally explained by reduction of thermally activated carrier trapping[82,83] and/or the electron-phonon coupling decrease.[27,83-87] One should note that the existence of "kink" has up to now only been reported with respect to the PL properties of QDs. Unusual "luminescence anti-quenching" at a well defined temperature of T~250 K (manifested in our experiments as "kink") has been observed for CdTe or CdSe/ZnS QDs initially dissolved in liquid solutions such as toluene, and has been related to a phase transition in the surfactant capping layer.[84] This phase transition of the surfactant was connected with surface relaxation and/or surface reconstruction which is strongly dependent on the type of capping ligand molecules (TOPO or aminoethanethiol) and, in turn, may cause a spatially-energetic reordering of trap states.

We have shown for the first time[55] that, in addition to PL, the QD band-edge absorption is obviously also sensitive to such a phase transition of the surfactant capping layer at temperatures close to ~218 K. When discussing the appearance of the "kink", one has to take into account that for TOPO- or amine-capped CdSe/ZnS QDs, a phase transition of the capping ligand layer at low T may cause some strain-induced deformation of the ZnS shell. The reason of that is that according to[88,89] absorption and PL of core-shell CdSe/ZnS QDs are red-shifted with respect to merely core QDs because in the former case the electron wave function tunnels into the shell, increasing the delocalization of the electron-hole pair, lowering the confinement energy and consequently the energy of the excited state. Correspondingly, due to different thermal expansion coefficients for the semi-rigid capping layer and the ZnS shell as well as possible strain effects, slight changes of electron delocalization may take
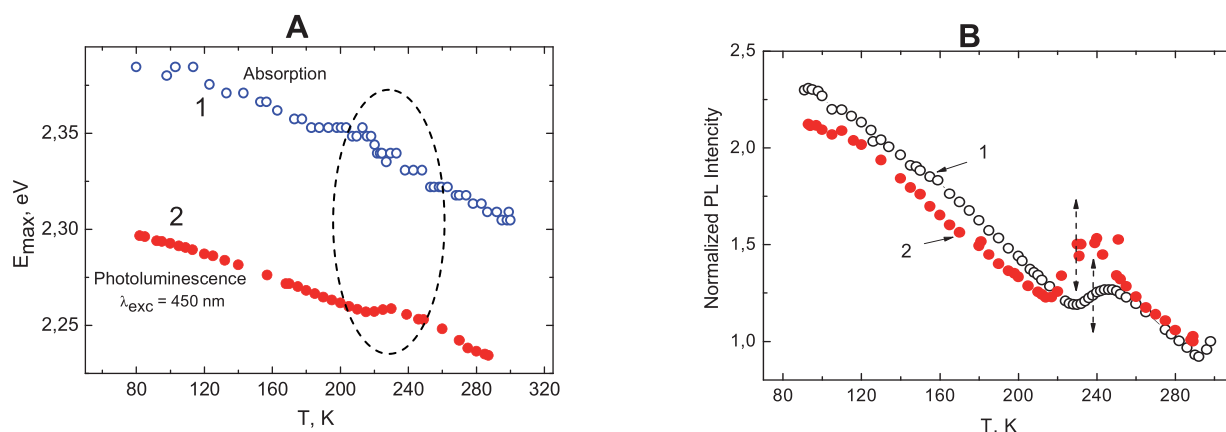

Figure 8. Temperature dependence of absorption and PL properties for alone QDs and "QD-Dye" nanocomposites in methylcyclohexane/toluene (6:1) mixture. *A*: Temperature dependence of (1) the first absorption peak (1, mean weighted data for two Gaussians lines) and PL maximum (2, λ_{exc}=450 nm) for TOPO capped CdSe/ZnS QDs (d_{CdSe} = 3.0 nm, 2 ZnS monolayers). Dashed ellipse indicates temperature range at which optical properties change. *B*: Temperature dependence of the normalized PL maximum intensity (λ_{exc}=450 nm) for CdSe/ZnS-AM QDs (d_{CdSe} = 3.0 nm, 2 ZnS monolayers) capped by long-chain amines (1) and for nanocomposites based on CdSe/ZnS-AM QDs and (pyridyl)$_2$-perylene diimide (DPP) dye molecules (see Figure 1B) at molar ratio x=[C_{DPP}]/[C_{QD}]=1 (2). Thick dashed arrows on the curves 1 and 2 indicate temperatures at which optical properties change.

place in the range of the phase transition. In this respect, we believe that slightly different "kink" temperatures for the first excitonic absorption band (~218 K) and the PL band (~223 K) for TOPO-capped CdSe/ZnS QDs, may be explained by the different nature of the corresponding transitions in absorption (allowed excitonic ones[55]) and in emission (trap dominated at low T).

If in fact, a trap state emission dominates at low temperatures, these trap states or their distribution might be influenced by dye molecules attached to the QD surface due to replacing some of the surfactant (TOPO ligand) molecules.[55,90] To realize such a situation we have carried out the corresponding temperature experiments for nanocomposites based on TOPO capped CdSe/ZnS QD of one type and various porphyrin molecules at a relative molar ratio of $x = [C_{porphyrin}]/[C_{QD}] = 1$ (Figure 9). In the case of CuP(*m*-Pyr)$_4$ being attached to QD, upon temperature lowering along with QD PL band, the long wavelength emission band at $\lambda_{max} = 770 \div 780$ nm appears (Figure 9A). The last emission belongs to the phosphorescence of CuP(*m*-Pyr)$_4$ molecules.[91 and references therein] It is clearly seen that this phosphorescence intensity is continuously increasing upon temperature lowering (Figure 9A, inset) what is typical for Cu-containing porphyrins.[91,92] Thus, CuP(*m*-Pyr)$_4$ molecules may be considered as an inner standard showing that the surrounding solvent matrix does not change upon temperature lowering At the same conditions, PL intensity for QD in "QD-CuP" nanocomposites shows again a "kink" (Figure 6A, inset), which, however, is now much more pronounced (-23%) than in the absence of CuP (compare curves 1 and 3, Figure 9B). A comparison of temperature dependent QD PL intensities obtained for various porphyrins is shown in Figure 9B. It is evident, that dye attachment enhances the PL decrease at the phase transition temperature, and the amplification is strongest for CuP molecules. We suggest that CuP exhibits the largest effect, since either internal molecular charge transfer states influence the energy distribution of CdSe/

ZnS QD trap states considerably or TOPO molecules may be strongly coordinated at low temperatures to the central Cu ion, which might increase the disorder of the surfactant capping shell. Finally, it is seen from Figure 9B (curve 4) that tetraphenylporphyrin without *meso*-pyridyl anchoring groups does not enlarge the QD PL decrease at the "kink" (because of self-assembly absence in this case), and the "kink" is absent for QDs in a dried rigid PMMA film on a quartz plate (curve 5). In the later case, the film rigidity suppresses the reorganization of the TOPO capping layer,[84] thus weakening a spatially-energetic reordering of QD trap states.

Figure 10 shows band-edge PL decays at various detection wavelengths within the QD PL band for TOPO capped CdSe/ZnS QDs (d_{CdSe} = 3.0 nm, 2 ZnS monolayers) and, as representative example, for "QD+CuP(*m*-Pyr)$_4$" nanocomposites (x=1) at 293 and 77 K. It is seen that the temperature-dependence of the PL decays is quite pronounced for QDs being alone (like in other cases[84]) and differs significantly from than found for in "QD-Porphyrin" nanocomposites. At 293 K PL decay for alone QDs is multiexponential at various detection wavelengths, and measured <τ> values do not change practically upon variation of detection wavelengths (Figure 10, curve 1). At 77 K QD PL decay is nonexponential in the short wavelength region, but at PL maximum and in the long wavelength region PL decay is monoexponential exclusively. In the later case, mean value <τ> is monotonically rising upon going to the long wavelength detection. It is evidently seen also that for the PL long wavelength region <τ> values at 77 K are noticeably higher relative to those measured at 293 K. In addition, at 295 K QD instantaneous spectra are the same practically at various delay times, while at 77 K the red shift of these spectra is observed upon increase of a registration delay time. Taken together, all these PL decay findings for alone QDs in a temperature range of 300÷77 K cannot be described by a thermal equilibrium between dark and bright excitonic states as far as such effects manifest
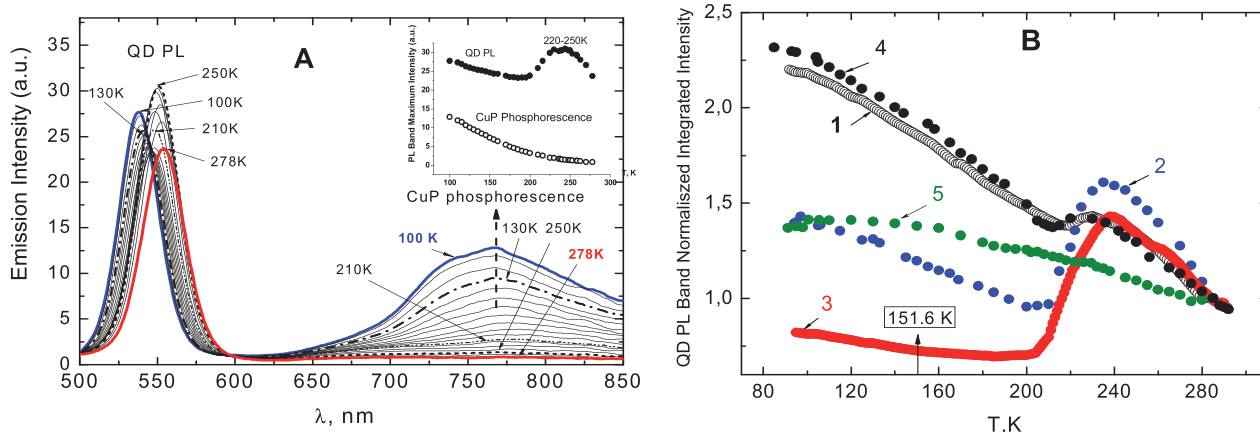

Figure 9. Temperature dependence of emission spectra (*A*) and band maxima intensities (B) for nanocomposites based on TOPO-capped CdSe/ZnS QDs and various porphyrin molecules at molar ratio $x=[C_{porphyrin}]/[C_{QD}]=1$ in methylcyclohexane/toluene (6:1) mixture (λ_{exc}=450 nm). The phase transition temperature of the solvent mixture is indicated by arrow. *A*: The short wavelength band belongs to QD PL, the increasing long wavelength band belongs to CuP(m-Pyr)$_4$ phosphorescence. The inset shows the temperature dependence for QD PL and CuP phosphorescence bands between 77 and 285 K. *B*: All curves are normalized to the integrated band intensity of QD PL at 285 K. Experimental temperature dependences are shown for the same type of CdSe/ZnS QD (d_{CdSe} = 3.0 nm, 2 ZnS monolayers) under various conditions and attached porphyrins: (1) alone QDs; (2) QD+H$_2$P(*m*-Pyr)$_4$; (3) QD+CuP(*m*-Pyr)$_4$; (4) QD+tetraphenylporphyrin (having no pyridyl rings); (5) QD in dried PMMA film on a quartz plate.
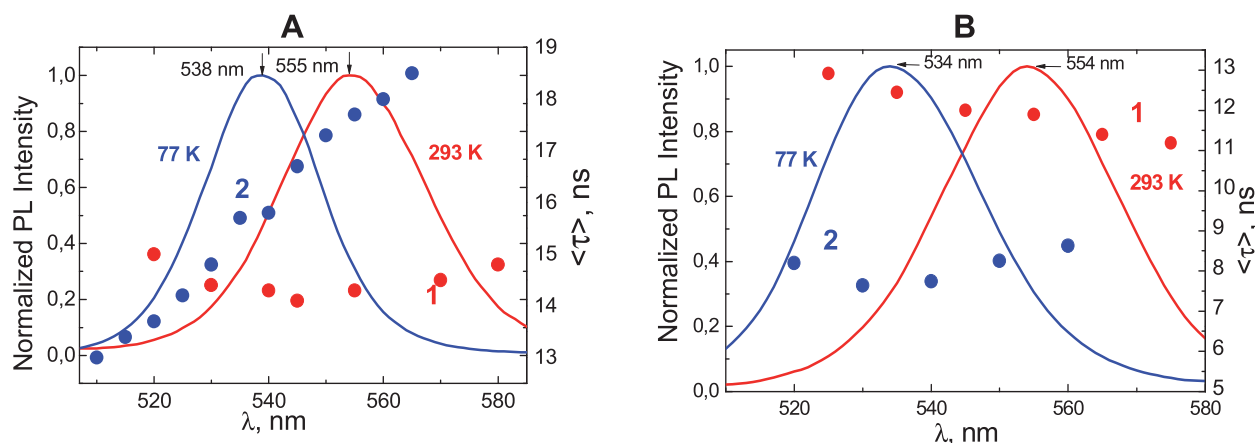
Figure 10. Dependence of the photoluminescence mean decay $\langle\tau\rangle$ on registration wavelength λ_{reg} for TOPO capped CdSe/ZnS QD (d_{CdSe} = 3.0 nm, 2 ZnS monolayers) at 293 (1) and 77 K (2) for alone QDs (A) and "QD+CuP(m-Pyr)$_4$" nanocomposites (at molar ratio x = 1) in methylcyclohexane/toluene (6:1) mixture. QD PL non-exponential decays $\langle\tau\rangle$ have been fitted by $I(t) = \Sigma A_i \cdot exp(-t/\tau_i)$ upon excitation at λ_{exc}= 410 nm, and the mean lifetime values have been calculated as $\langle\tau\rangle = \Sigma(A_i \cdot \tau_i^2) / \Sigma(A_i \cdot \tau_i)$.

themselves at T < ~ 50 K.[84,93] The realistic mechanisms of exciton relaxation in this case may be dominated by trapping dynamics, since the trap depths vary across the QD ensemble and also fluctuate in time for individual QDs.[94]

In the case of "QD+CuP(m-Pyr)$_4$" nanocomposites, QD PL decays are multiexponential within the whole PL band both at room and low temperature (Figure 10B), and measured <τ> values slightly change upon variation of detection wavelengths. At 293 K, the mean decay shortening from <τ>≈14.5 ns for alone QDs down to <τ>≈11.9 ns for nanocomposites is a direct evidence of OD PL quenching in nanocomposites due to both the electron tunneling and FRET. At 77 K, PL spectra of nanocomposites are blue shifted with respect to those for individual QD that may be considered as an additional support reflecting the influence of attached CuP molecule on QD phase transition. Data presented in Figure 10 show also that in contrast to alone QDs, the temperature lowering down to 77 K leads to the strong shortening of mean <τ> values even for the PL long wavelength region (from ~18 ns down to ~8 ns). The interpretation of these results is also connected with TOPO capping layer phase transition perturbed by attached porphyrin molecules. The existence of additional PL quencher (attached CuP molecules) in this case may influence non-directly on the relative position of excitonic and trap states of QD itself upon temperature lowering as well as form the competitive non-radiative channels connected with CuP(m-Pyr)$_4$ molecules.

To consider the differences in the temperature dependence between QDs and nanoassemblies, one has to take into account that nanoassemblies at an initial molar ratio $x = [C_{CuP}]/[C_{QD}]$ = 1 were prepared by one-step mixing at ambient temperature. At ambient temperature, the thermodynamic formation of such self-aggregated assemblies is characterized by the corresponding complexation constant. [49,76] Estimations according to a Poisson distribution show that at x=1, the related probabilities P_i of the number of dye molecules per QD are P_0=0.3, P_1=0.4, P_2=0.3, respectively. This implies, that some QDs are "porphyrin-free" without PL

quenching at ambient temperature. Decrease of temperature leads probably to complete complexation of QDs because of the rise of the complexation constant at low temperatures.[95] Correspondingly, this should show up in more effective QD PL quenching.

Thus, the combined analysis of QD PL integrated intensities the decay curves for alone QDs and "QD-Porphyrin" nanocomposites leads to the conclusion that upon temperature lowering, QD undergo a phase transition in the sense, that the "freezing" ligand shell exerts strain on the ZnS shell thus creating trap states with reduced PL quantum yields. Moreover, this phase transition changes also the CdSe core absorption, which might be explained by a modification of the core structure. In turn, dye attachment creates new and/or more trap states, which obviously quench the PL very effectively. Phase transition temperature and the influence of dye (porphyrins or perylene diimides in our study) induced trap states depend critically on the type of the capping ligand and are more pronounced for TOPO as compared to long chain amines.[55] We have demonstrated in this section, that dye molecules (porphyrins or perylene diimides in our study) noticeably influence the optical properties at ligand controlled phase transitions. Our findings highlight that single functionalized heterocyclic molecules can be considered as extremely sensitive probes for the complex interface physics and dynamics of colloidal semiconductor QDs.

PL Blinking Statistics for QDs with Attached Porphyrins and Long-Term Photostability of Single CdSe/ZnS QDs and Nanocomposites

At present, it is well-documented that the photoluminescence from a variety of single organic molecules[96] and colloidal semiconductor QDs[97] is defined by large intensity fluctuations, known as "blinking", whereby their PL turns "on" and "off" intermittently, even under continuous photoexcitation. This is an intriguing phenomenon as it results in a clearly measurable manifestation of
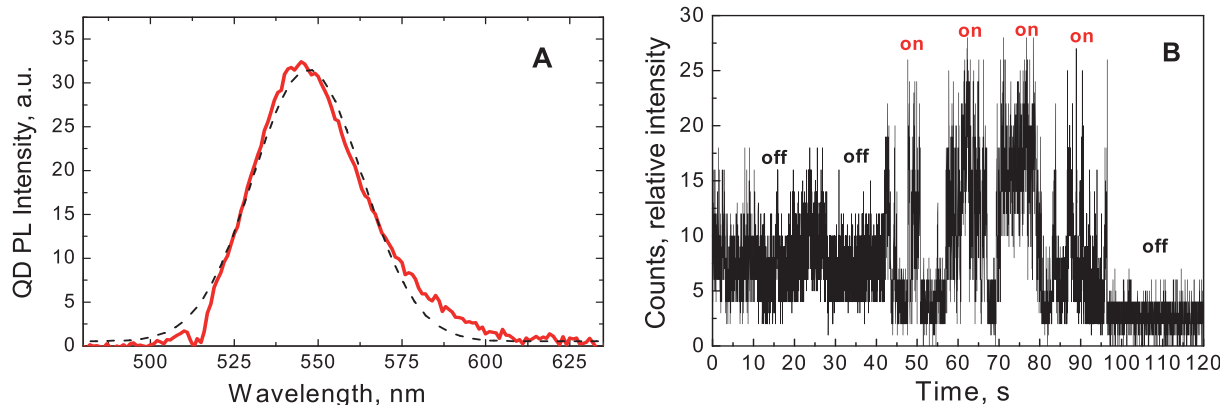
Figure 11. PL spectrum (*A*), and "on" and "off" intensity fluctuations (blinking) for single TOPO capped CdSe/ZnS QD (*B*) in polystyrene film (*C*~10⁻¹¹ M⁻¹) on quartz plate at 295 K. QD parameters: d_{CdSe} = 3.2 nm, 3 ZnS monolayers; laser excitation at λ_{exc} = 514.5 nm, P=2.5 μW. The dashed curve in (A) presents a Gaussian fit of the PL band.
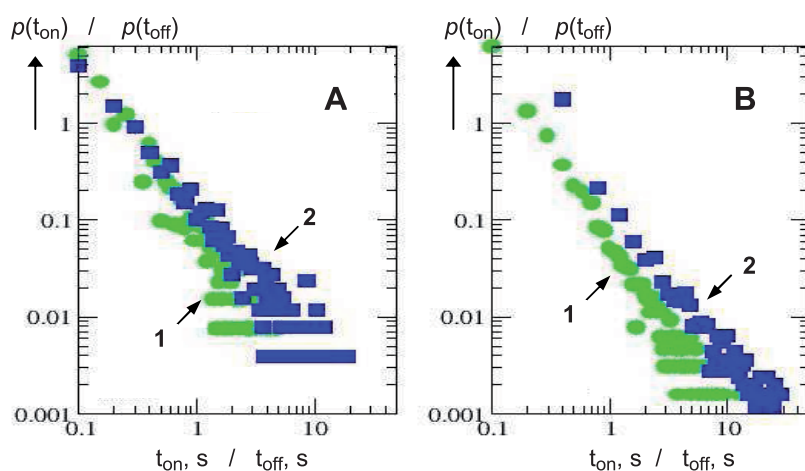

Figure 12. Blinking statistics for single TOPO capped CdSe/ZnS QDs (*A*) and for single "QD+H$_2$P(*m*-Pyr)$_4$" nanocomposites at molar ratio *x* = 10 (*B*). QD parameters: d_{CdSe} = 3.2 nm, 3 ZnS monolayers; laser excitation at λ_{exc} = 514.5 nm, P=250 μW. Samples have been prepared by spin coating from toluene solution onto quartz surface at 295K. The presented data were averaged for at least 20 individual objects from free and porphyrin-assembled QDs. Average on- (1, green) and off-times (2, blue) are indicated in each graph.

microscopic dynamical changes in a single object (molecule or QD).[98] In most cases the durations of bright ("on") and dark ("off") periods (PL time trajectories) follow power-law statistics:[97,98]

$$p(\tau) \sim \tau^{-\mu} \qquad (5),$$

where τ is the observation time, μ is an exponent index changing within 1.1÷2.2 s with a maximum at ~1.5 s. The power-law behaviour holds regardless of sample temperature, QD size or composition, QD shape, or excitation intensity.

PL intensity fluctuations of blinking QDs occur on wide time scales (Figure 11) which are immensely longer than the longest characteristic time normally associated with QD dynamics, a radiative lifetime of tens of nanoseconds. [97,98] Hence, they must be associated with "slow" variations of the microscopic state of the QD caused by changed of interface properties (*e.g.* capping layer phase transition or dye molecule attachment, like in our case).

As we discussed in previous sections, the attachment of functionalized organic dyes (porphyrins or perylene diimides) to a QD surface manifests itself in noticeable

QD PL quenching as well as in related complex interface dynamics.

A modification of QD PL properties is also visible in the experiments with single "QD-Porphyrin" nanocomposites. Figure 12 shows the comparison of blinking statistics for two samples spin coated from toluene solution onto quartz surface at 295 K: TOPO-capped CdSe/ZnS QDs and "QD-H$_2$P(*m*-Pyr)$_4$" nanocomposites both having the same initial QD concentration (C_{QD}=1.8·10⁻⁹ M, core diameter d_{CdSe} = 3.2 nm, 3 ZnS monolayers) and being excited within the QD first absorption band. Nanoassemblies were prepared at a molar ratio *x* = [$C_{Porphyrin}$]/[C_{QD}] = 10, at which the ensemble QD PL quenching is about 40%.[46] It is seen from Figure 12 that for both single QDs and single nanocomposites blinking statistics show a power law distribution for "on" and "off" times. Dark QD states are usually explained by charged QDs,[99] and the heterogeneity (power law behavior) is inherent to broadly distributed (de-)population processes of the dark state.

It was found that <t_{on}> times of 0.20 s are the same in QDs and "QD-H$_2$P(*m*-Pyr)$_4$" nanocomposites. In contrast, a substantial increase of <t_{off}> times is observed for
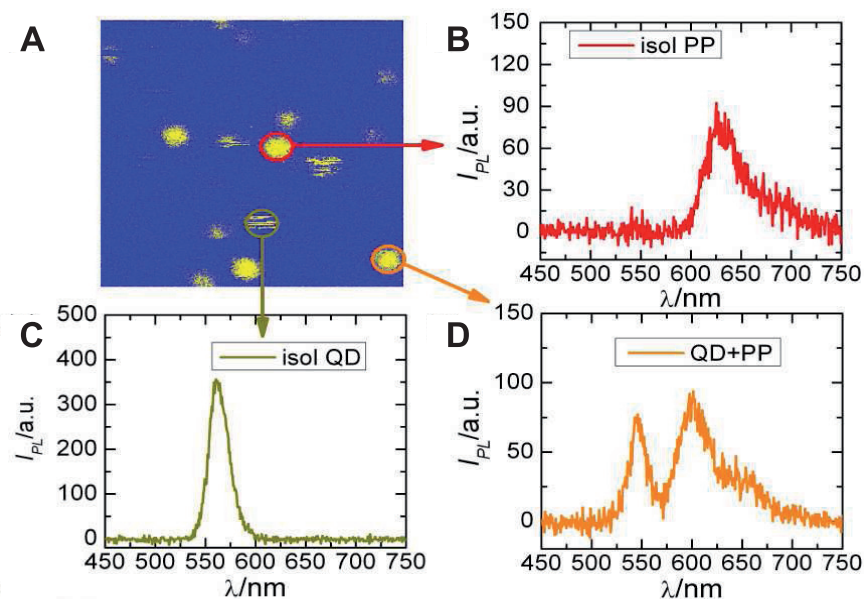
Figure 13. *A*: 5×5 μm² confocal scan (λ_{exc} = 465 nm; P = 0.6 kW·cm⁻²) of the photoluminescence for single objects based on long-chain amines capped quantum dot (QD-AM, d_{CdSe} = 3.0 nm, 2 ZnS monolayers) and (pyridyl)₁-perylene diimide (PP) molecules at *x* = 1 (see Figure 1B). Apparent stripes indicate blinking processes. Because of Poisson distribution of dye molecules on QDs it was possible to detect PL spectra (1 s binning time) of single PP (*B*), single QD-AM (C) and single nanocomposite with colocolized PP and QD-AM (*D*).

nanocomposites (<t_{off}>=1.2 s) in comparison to <t_{off}>=0.75 s for QDs. These findings are considered as a proof of QD-porphyrin interactions leading to changed QD PL dynamics also on a single assembly level.

At the end, as an additional example of single objects experiments on "QD-Dye" nanocomposites, we show some results being obtained for quantum dots capped by long-chain amines (QD-AM, d_{CdSe}= 3.0 nm, 2 ZnS monolayers) and at-tached with (pyridyl)₁-perylene diimide (PP) molecules. With respect to porphyrins, perylene diimides are more suitable for single molecule detection due to their high quantum yield of fluorescence and large photostability.[51,52,70,71,100] With these investigations it seems to be possible to elaborate a microscopic description of the geometry and dynamics of QD-dye nanoassemblies. Additionally, a comparison of ensemble and single assembly experiments allows the unravelling of PL specific quenching mechanisms which are of importance for the identification of dynamic processes in QD-dye nanocomposites in general.

Figure 13A shows a confocal scan of a spin-coated sample based on long-chain amines capped quantum dot (QD-AM, d_{CdSe} = 3.0 nm, 2 ZnS monolayers) and (pyridyl)₁-perylene diimide (PP) molecules at *x* = 1 (the corresponding structure is presented in Figure 1B). Detecting the luminescence spectra on each single luminescent spot reveals that three types of spectroscopic fingerprints emerge: (i) PP fluorescence spectra (Figure 13B); (ii) QD-AM PL spectra (Figure 13C) and (iii) simultaneous QD-AM and PP spectra belonging to a nanocomposite (Figure 13D). The detection of these three types of emission is an experimental background of the distribution of dye molecules on QDs which may be described by Poisson approach. Moreover, the spectral shift of PP emission in (D) with respect to (B) is due to different conformations of PP molecules on QD surface[100] (see Figure 1B).

PL spectra of a single (QD-AM)-PP nanocomposite as a function of observation time and QD-AM kinetic properties are presented in Figure 14. It is evidently seen that at t ≈ 57 s PP fluorescence is bleached while QD-am remains emitting because of higher photostability in comparison with an organic dye (Figure 14A). In addition, PL band of this quantum dot is blue shifted upon the observation time increase. While the fluorescence of single PP molecules decays almost mono-exponentially, the PL of single QD-AM (independent whether free or assembled) decays clearly multi-exponential as has been reported for many similar cases.[101-103] It should be noted also that photoluminescence average decay times ⟨τ_D⟩ of single QD-AM (fitted by a stretched exponent) show a tendency to decrease with increasing observation time, and this behaviour seems to be related to the spectral blue shift of PL band. Average decay time for single uncomplexed QD-AM was measured to be ⟨τ_D⟩≈20.5ns (based on measurements for 20 QDs), while for QD in single nanocomposite (QD-AM)- PP ⟨τ_{DA}⟩≈16 ns (based on measurements for 18 nanocomposites). The shortening of the decay time is clearly related to the observed decrease of the QD PL intensity upon nanocomposite formation. This proves that QD PL quenching is also observed on a single nanoassembly level and reflects directly the existence of an additional non-radiative channel for QD exciton relaxation in this nanocomposite.

Finally, let us consider the specific effects which may be detected using single nanocomposite detection. Figure 15A shows the PL spectrum of single amine capped QD–AM (only QD PL spectrum in one focal laser spot) in a time trace of the PL intensity during 60 s with 1 s resolution. We observe besides blinking a small blue shift. In Figure 15B the superposition of QD-AM and (pyridyl)₁-perylene diimide (PP) emission (within one laser spot) shows a stable fluores-cence of PP (at λ=600 nm), while the PL of the QD-AM (at
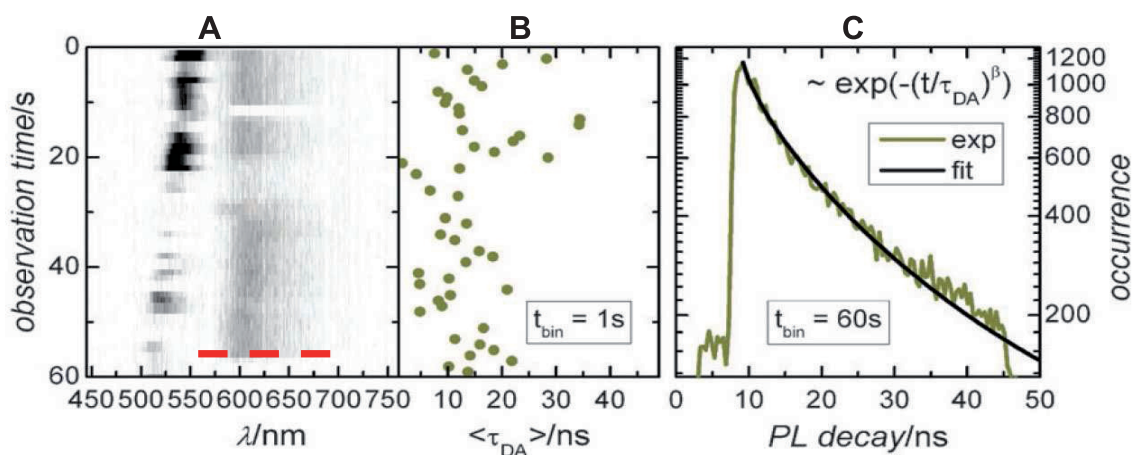
Figure 14. Temporal spectral and kinetic properties of a single (QD-AM)-PP nanocomposite.[52] *A*: PL spectra are shown as a function of observation time (λ_{exc} = 465 nm; P = 0.6 kW·cm⁻²). At t ≈ 57 s PP fluorescence is bleached (shown by red dashed line). *B*: Related PL decay times $\langle \tau_{DA} \rangle$ for QD-AM obtained from a stretched exponential fit as a function of the observation time. *C*: PL decay of QD-AM in the assembly accumulated over an observation time of 60 s. The full line shows a fit to a stretched exponential function.
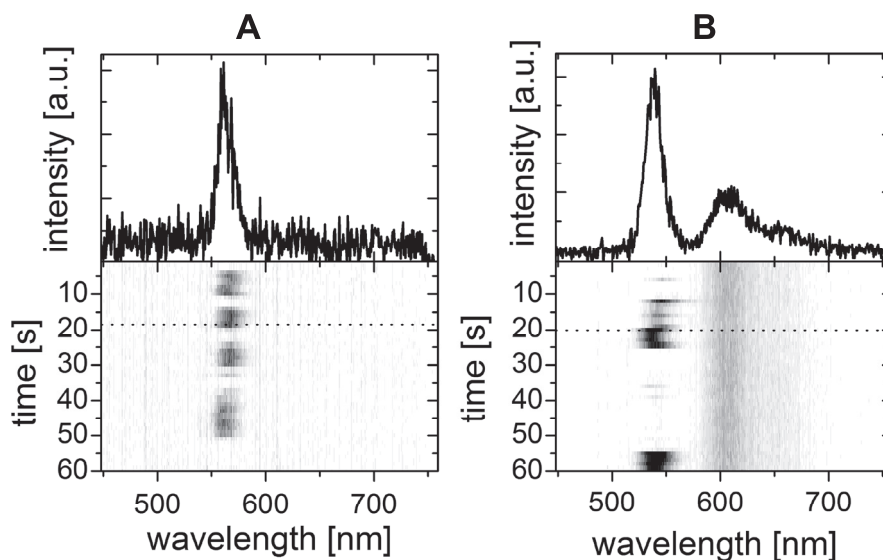

Figure 15. Top: Photoluminescence spectrum of single CdSe/ZnS QD-AM (*A*) and emission spectrum of a single CdSe/ZnS QD-AM and a single (pyridyl)₁-perylene diimide (PP) molecule forming a nanocomposite at molar ratio *x*=1 (*B*) at ambient temperature. Bottom: Luminescence intensities and wavelengths as a function of observation time. The broken lines show actually the frame (time) where the spectrum shown above is taken from. Time resolution is 1 s. Single QDs and nanocomposites were excited with a repetition rate of 10 MHz at λ=465 nm on the timescale of minutes with constant average excitation power of approximately 400 W/cm².

λ=560 nm) is blinking and blue shifting more effectively than in the absence of PP. In fact, the PL of quantum dots with attached PP molecules shifts more effectively (by ~25 nm) to the blue than the PL of free single QDs (~17 nm).[55]

The overall conclusion with respect to "QD-Dye" nanocomposites is that there is a noticeable difference in the photophysical behaviour of QD PL upon the dye attachment. Single particle detection indicates that even one attached PP molecule enhances the photodegradation considerably. With respect to the photodegradation, two reasons may be tentatively taken into account. The first one is that upon attachment of dye molecules a large number of ligands are removed, which results in a more unprotected and thus more reactive surface, which allows for a stronger photodegradation either of surface states or even of the QD core. The second reason is related to the fact, that dye–induced trap states of QDs are more sensitive to photobleaching resulting in apparent spectral shifts and reduced integrated PL. This latter assumption is supported by our experiments on "QD-porphyrin" nanocomposites reported in previous sections of the paper.

Conclusions

Our recent findings highlight that "bottom-up" approach based on self-assembly principles defines the strategy of the formation of organic-inorganic nanocomposites containing colloidal semiconductor QDs of different types

and various heterocyclic molecules with specific anchoring side substituents (like *meso*-pyridyl substituted porphyrins and perylene diimides in our case). On the basis of a combination of ensemble and single molecule spectroscopy of nanocomposites, we have shown that single functionalized molecules can be considered as extremely sensitive probes for studying the complex interface physics and exciton relaxation processes in QDs.

We have quantitatively discriminated for the first time, that the major part of the observed QD PL strong quenching in nanocomposites can be understood in terms of the electron tunneling across the ZnS shell in the conditions of quantum confinement, and the rest part of the quenching is caused by FRET. The temporal QD PL quenching induced by attaching dye molecules can be explained by the presence of a limited number of empty quencher sites on the QD surface followed by ligand competitive exchange (TOPO, amines and dyes) on much slower time scales. We like to emphasize that also at these long time scales a still increasing attachment of $H_2P(m\text{-}Pyr)_4$ molecules as identified by further increasing FRET has been observed. Our present findings of inhomogeneous surface dynamics for semiconductor QDs are also important for the evaluating the mechanisms non-FRET quenching processes caused by attachment of dye molecules. We have argued that non-FRET quenching might be related to depletion of capping ligand molecules by the respective dye molecules. Using porphyrins and perylene diimides attaching with QD surface, we did a conclusion that this non-FRET mechanism could be related to the inhomogeneity of the QD surface with respect to ligand attachment. In case that there are various attachments sites with varying binding strengths it is reasonable to assume that different attachment sites are correspondingly related to a formation of trap states which quench the QD PL effectively. Summarizing all these arguments, non-FRET quenching corresponds to the removed of ligands at specific surface sites and the creation of (PL quenching) trap states. Hence, for this tuning the PL properties, it does not need a full exchange of the ligand shell, but it works already upon attachment of very few dye molecules.

Temperature variation and related changes in QD absorption and emission reveal sharp changes of the ligand shell structure in a narrow temperature range for organic (TOPO and amine) surfactants (phase transition). The effects on QD PL at this transition become considerably pronounced upon attachment of only a few porphyrin (or perylene diimide) molecules to QD surface. We conclude from temperature experiments, that the ligand phase transition has impact on the QD core structure and exciton-phonon coupling. This investigation elaborates the importance of (switchable) surface states for the characterization of the PL of QDs.

Finally we like to point out, that properties of QD-dye nanocomposites are interesting in itself, but also provide a valuable tool to study surface related phenomena in QDs on an extremely low level of the surface modification. Instead of investigating the exchange ligand dynamics directly *e.g.* by NMR, we suggest to make use of QD PL quenching in combination with appropriately functionalized dye molecules. In contrast to NMR, this approach allows to investigate ligand dynamics at extremely low concentrations of concurrent ligand-type dyes. At last, our data show also, that "QD-Porphyrin" nanocomposites may be considered as

potential photosensitizers of a novel type in the photodynamic therapy of cancer.

References

1. Hirst A.R., Escuder B., Miravet J.F., Smith D.K. *Angew. Chem., Int. Ed.* **2008**, *47*, 8002-8018, and the references therein.
2. Zhang L., Webster T.J. *Nano Today* **2009**, *4*, 66-80.
3. Moyano D.F., Goldsmith M., Solfiell D.J., Landesman-Milo D., Miranda O.R., Peer D., Rotello V.M. *J. Am. Chem. Soc.* **2012**, *134*, 3965-3967.
4. De Mello Donega C. *Chem. Soc. Rev.* **2011**, *40*, 1512-1546.
5. Talapin D.V., Lee J.-S., Kovalenko M.V., Shevchenko E.V. *Chem. Rev.* **2010**, *110*, 389-458.
6. Mocatta D., Cohen G., Schattner J., Millo O., Rabani E., Banin U. *Science* **2011**, *332*, 77-81.
7. Liang G.-X., Li L.-L., Liu H.-Y., Zhang J.-R., Burda C., Zhu J.-J. *Chem. Commun.* **2010,** *46*, 2974-2976.
8. Cheng H.-M. *Chem. Commun.* **2011**, *47*, 6763-6783.
9. Whitesides G.M., Grzybowski B. *Science* **2002**, *295*, 2418-2421.
10. Unterkofler S., Pflock T., Southall J., Cogdell R.J., Koehler J. *ChemPhysChem* **2011**, *12*, 711-716.
11. Freiberg A., Trinkunas G. In: *Unraveling the Hidden Nature of Antenna Excitations* (Laisk A., Nedbal L., Govindjee, Eds.). Amsterdam: Springer Science+Media B.V., **2009**, p. 55-82.
12. Special Issue on "Supramolecular Approaches to Organic Electronics and Nanotechnology" *Adv. Mater*. **2006**, *18*, 1227-1329.
13. Mansoori G.A. *Principles of Nanotechnology. Molecular-Based Study of Condensed Matter in Small Systems.* Chicago: University of Illinois at Chicago, USA, **2005**.
14. Nicolini C. Nanoscale Materials. In: *Nanotechnology and Nanobiosciences*. Pan Stanford Series on Nanobiotechnology, **2010**, Vol. 1, Ch. 1.
15. Zenkevich E.I., von Borczyskowski C., Shulga A.M. *J. Porphyrins Phthalocyanines* **2003**, *7*, 731-754.
16. Maligaspe E., Kumpulainen T., Lemmetyinen H., Tkachenko N.V., Subbaiyan N.K., Zandler M.E., D'Souza F. *J. Phys. Chem., A* **2010**, *14*, 268-277.
17. Lee J.-E., Yang, J., Gunderson V.L., Wasielewski M.R., Kim D. *J. Phys. Chem. Lett.* **2010**, *1*, 284-289.
18. Sagun E.I., Zenkevich E.I., Knyukshto V.N., Shulga A.M. *Opt. Spectrosc.* **2011**, *110*, 242-255.
19. Liu J.-Y., El-Khouly M.E., Fukuzumi S., Ng D.K.P. *Chem.– Eur. J.* **2011**, *17*, 1605-1613.
20. Zenkevich E.I., von Borczyskowski C. Photoinduced Relaxation Processes in Self-assembled Nanostructures:

Multiporphyrin Complexes and Composites "CdSe/ZnS Quantum Dot-Porphyrin. In: *Multiporphyrin Arrays: Fundamentals and Applications* (Kim D., Ed.). Singapore: Pan Stanford Publishing Pte. Ltd., **2011**, p. 217-288.

21. Bottari G., Suanzes J.A., Trukhina O., Torres T. *J. Phys. Chem. Lett*. **2011**, *2*, 905-913.

22. Sakurai T., Tashiro K., Honsho Y., Saeki A., Seki S., Osuka A., Muranaka A., Uchiyama M., Kim J., Ha S., Kato K., Takata M., Aida T. *J. Am. Chem. Soc*. **2011**, *133*, 6537-6540.

23. Colvin M.T., Ricks A.B., Scott A.M., Smeigh A.L., Carmieli R., Miura T., Wasielewski M.R. *J. Am. Chem. Soc*. **2011**, *133*, 1240-1243.

24. Medforth C.J., Wang Z., Martin K.E., Song Y., Jacobsen J.L., Shelnutt J.A. *Chem. Commun*. **2009**, 7261-7277.

25. Kim F.S.; Ren G., Jenekhe S.A. *Chem. Mater*. **2011,** *23*, 682-732.

26. Xu H., Ermilov E.A., Röder B., Ng D.K.P. *Phys. Chem. Chem. Phys*. **2010**, *12*, 7366-7370.

27. Klimov V. In: *Handbook of Nanostructured Materials and Nanotechnology*. (Nalwa H.S., Ed.). USA: Acad. Press, **2000**, Vol. 4, p. 451-527.

28. Woggon U. *Optical Properties of Semiconductor Quantum Dots*. Berlin: Springer, **2006**.

29. *Semiconductor Nanocrystal Quantum Dots: Synthesis, Assembly, Spectroscopy and Applications*. (Rogach A.L., Ed.). Wien: Springer-Verlag, **2008**.

30. Gaponenko S.V. *Introduction to Nanophotonics*. Cambridge: Cambridge University Press, **2010**.

31. Coe-Sullivan S., Woo W.-K., Steckel J.S., Bawendi M., Bulovic V. *Organic Electronics* **2003**, *4*, 123-130.

32. Wang M., Moon S.-J., Xu M., Chittibabu K., Wang P., Cevey-Ha N.-L. Humphry-Baker R., Zakeeruddin S. M., Graetzel M. *Small* **2010**, *6*, 319-324.

33. Medintz I.L., Stewart M.H., Trammell S.A., Susumi K., Delahanty J.B., Mey B.C., Melinger J.S., Blanco-Canosa J.B., Dawson F.E., Mattoussi H. *Nature Materials* **2010**, *9*, 676-684.

34. Frasco M.F., Chaniotakis N. *Sensors* **2009**, *9*, 7266-7286.

35. Hetsch F., Xu X., Wang H., Kershaw S.V., Rogach A.L. *J. Phys. Chem. Lett*. **2011**, *2*, 1879-1887.

36. Erdogmus A., Moeno S., Litwinski Ch., Tebello N. *J. Photochem. Photobiol., A* **2010**, *210*, 200-208.

37. De M., Ghosh P.S., Rotello V.M. *Adv. Mater*. **2008**, *20*, 4225-4241.

38. Orlova A.O., Gubanova M.S., Maslov V.G., Vinogradova G.N., Baranov A.V., Fedorov A.V., Gounko L. *Optika i Spektroskopiya* **2010**, *108*, 975-882 (in Russ.).

39. Chernook A.V., Shulga A.M., Zenkevich E.I., Rempel U., von Borczyskowski C. *J. Phys. Chem*. **1996**, *100*, 1918-1926.

40. Chernook A.V., Rempel U., von Borczyskowski C., Zenkevich E.I., Shulga A.M. *Chem. Phys. Lett*. **1996**, *254*, 229-241.

41. Bachilo S.M., Willert A., Rempel U., Shulga A.M., Zenkevich E.I., von Borczyskowski C. *J. Photochem. Photobiol., A* **1999**, *126*, 99-109.

42. Zenkevich E.I., Willert A., Bachilo S.M., Rempel U., Kilin D.S., Shulga A.M., von Borczyskowski C. *Mater. Scie. Eng., C* **2001**, *18*, 99-111.

43. Zenkevich E.I., von Borczyskowski C., Shulga A.M., Bachilo S.M., Rempel U., Willert A. *Chem. Phys*. **2002**, *275*, 185-209.

44. Sagun E.I., Zenkevich E.I., Knyukshto V.N., Shulga A.M., Starukhin D.A., von Borczyskowski C. *Chem. Phys*. **2002**, *275*, 211-237.

45. Sagun E.I., Zenkevich E.I., Knyukshto V.N., Shulga A.M., Ivashin N.V. *Opt. Spectrosc*. **2010**, *108*, 590-607.

46. Zenkevich E., Cichos F., Shulga A., Petrov E., Blaudeck T., von Borczyskowski C. *J. Phys. Chem., B* **2005**, *109*, 8679-8692.

47. Kilin D.S., Tsemekhman K., Prezhdo O.V., Zenkevich E.I., von Borczyskowski C. *J. Photochem. Phobiol., A* **2007**, *190*, 342-354.

48. Blaudeck T., Zenkevich E., Cichos F., von Borczyskowski C. *J. Phys. Chem., C* **2008**, *112*, 20251-20257.

49. Zenkevich E.I., von Borczyskowski C. *Macroheterocycles* **2009**, *2*, 57-71.

50. Zenkevich E.I., von Borczyskowski C. *High Energy Chem*. **2009**, *43*, 570-576.

51. Kowerko D., Krause S., Amecke N., Abdel-Mottaleb M., Schuster J., von Borczyskowski C. *Int. J. Mol. Sci*. **2009**, *10*, 5239-5256.

52. Kowerko D., Schuster J., Amecke N., Abdel-Mottaleb M., Dobrawa R., Wuerthner F., von Borczyskowski C. *Phys. Chem. Chem. Phys*. **2010**, *12*, 4112-4123.

53. Zenkevich E.I., Sagun E.I., Knyukshto V.N., Stasheuski A.S., Galievsky V.A., Stupak A.P., Blaudeck T., von Borczyskowski C. *J. Phys. Chem., C*. **2011,** *115*, 21535-21545.

54. Blaudeck T., Zenkevich E., Abdel-Mottaleb M., Szwaykowska K., Kowerko D., Cichos F., von Borczyskowski C. *ChemPhysChem* **2011,** *13*, 959-972.

55. Zenkevich E.I., Stupak A.P., Kowerko D., von Borczyskowski C. *Chem. Phys*. **2012** (DOI: 10.1016/j.chemphys.2012.02.008).

56. Yarovoi A.A., Zenkevich E.I., Sagun E.I., Knyukshto V.N., Shulga A.M., Stupak A.P., Dubovskii V.L. *Proc. SPIE* **2007**, *6728*, 67282K.

57. Zenkevich E. I., Sagun E.I., Yarovoi A.A., Shulga A.M., Knyukshto V.N., Stupak A.P., von Borczyskowski C. *Opt. Spectrosc*. **2007**, *103*, 958-968.

58. Frasco M.F.; Vamvakaki, V.; Chaniotakis, N. *J. Nanopart. Res*. **2009**, 6, 1501-1507.

59. Qi Z-D., Li D-W., Jiang P., Jiang F-L., Li Y-S., Liu Y., Wong W-K., Cheah K.-W. *J. Mater. Chem*. **2011**, *21,* 2455-2458.

60. Tsay J.M., Trzoss M., Shi L., Kong X., Selke M., Jung M.E., Weiss S. *J. Am. Chem. Soc*. **2007**, *129*, 6865-6871.

61. Rakovich A., Rakovich T., Kelly V., Lesnyak V., Eychmuller A., Rakovich Y. P., Donegan J.F. *J. Nanoscie. Nanotechnol*. **2009**, *9*, 1-7.

62. Clapp R., Medintz I.L., Mattoussi H. *ChemPhysChem* **2006**, *7*, 47-57.

63. Schmelz O., Mews A., Basche T., Herrmann A., Muellen K. *Langmuir* **2001**, *17*, 2861-2865.

64. Dayal S., Burda C. *J. Am. Chem. Soc*. **2007**, *129*, 7977-7981.

65. Ren T., Mandal, P. K., Erker W., Liu Z., Avlasevich Y., Puhl L., Müllen K., Basché T. *J. Am. Chem. Soc*. **2008**, *130*, 17242-17243.

66. Bullen C., Mulvaney P. *Langmuir* **2006**, *22*, 3007-3013.

67. von Holt B., Kudera S., Weiss A., Schrader T., Manna L., Parak W.J., Braun M. *J. Mater. Chem*. **2008**, *18*, 2728-2732.

68. Frenzel J., Joswig J.-O., Seifert G. *J. Phys. Chem., C* **2007**, *111*, 10761-10770.

69. Knowles K.E., McArthur E.A., Weiss E.A. *ACS Nano* **2011**, *5*, 2026-2035.

70. Dobrawa R., Würthner F. *Chem. Commun*. **2002**, 1878-1879.

71. Lang E., Würthner F., Köhler J. *ChemPhysChem* **2005**, *6*, 935-941.

72. Marcus Y. *Solvent Mixtures*. New York: Marcel Dekker, **2002**.

73. Tachiya M. *J. Chem. Phys. Lett*. **1982**, *76*, 340-348.

74. Song N., Zhu H., Jin S., Zhan W., Lian T. *ACS Nano* **2011**, *5*, 613-621.

75. Knowles K.E., Frederick M.T., Tice D.B., Morris-Cohen A.J., Weiss E.A. *J. Phys. Chem. Lett*. **2012**, *3*, 18-26.

76. Zenkevich E.I., Blaudeck T., Shulga A.M., Cichos F., von Borczyskowski C. *J. Lumin*. **2007**, *122-123*, 784-788.

77. Lakowicz J.R. *Principles of Fluorescence Spectroscopy*. New York: Kluwer Academic/Kluwer Publishers, 2nd edition, **1999**.

78. Zenkevich E.I., Blaudeck T., Abdel-Mottaleb M.M.S., Cichos F., Shulga A.M., von Borczyskowski C. *Int. J. Photoenergy* **2006**, ID 90242.

79. Voznyy O. *J. Phys. Chem., C* **2011**, *115*, 15927-15932.

80. Munro A.M., Jen-La Plante I., Ng M.S., Ginger D.S. *J. Phys. Chem., C* **2007**, *111*, 6220-6227.

81. Petrov E.P., Cichos F., von Borczyskowski C. *J. Lumin.* **2006**, *119-120*, 412-417.

82. Dayal S., Burda C. *J. Am. Chem. Soc.* **2007**, *129*, 7977-7981.

83. Morello G., De Giorgi M., Kudera S., Manna L., Cingolani R., Anni M. *J. Phys. Chem., C.* **2007**, *111*, 5846-5849.

84. De Mello Donega C., Bode M., Meijerink A. *Phys. Rev. B: Condens. Matter Mater. Phys.* **2006**, *74*, 085320/1-085320/9.

85. Liptay T.J., Marshall L.F., Rao P.S., Ram R.J., Bawendi M.G. *Phys. Rev. B: Condens. Matter Mater. Phys.* **2007**, *76*, 155314.

86. Liptay T.J., Ram R.J. *Appl. Phys. Lett.* **2006**, *89*, 223132.

87. Fernee M.J., Littleton B.N., Cooper S., Rubinsztein-Dunlop H., Gomez D.E., Mulvaney P. *J. Phys. Chem., C* **2008**, *112*, 1878-1886.

88. Peng X., Schlamp M.C., Kadavanich A.V., Alivisatos A.P. *J. Am. Chem. Soc.* **1997**, *19*, 7019-7029.

89. Dabbousi B.O., Redriguez-Vejo J., Mikulec F.V., Heine J.R., Mattousi H., Ober R., Jensen K.F., Bawendi M.G. *J. Phys. Chem., B* **1997**, *101*, 9463-9475.

90. Kaluzhny G., Murray R.W. *J. Phys. Chem., B* **2005**, *109*, 7012-7021.

91. Zenkevich E.I., von Borczyskowski C. Multiporphyrin Self-assembled Arrays in Solutions and Films: Thermodynamics, Spectroscopy and Photochemistry. In: *Handbook of Polyelectrolytes and Their Applications* (Tripathy S.K., Kumar J., Nalwa H.S., Eds.). USA: Amer. Sci. Publ., **2002**, Vol. 2., p. 301-348.

92. Kim D., Holten D., Gouterman M. *J. Am. Chem. Soc.* **1984**, *106*, 2793-2798.

93. Klimov V. *Annu. Rev. Phys. Chem.* **2007**, *58*, 635-673.

94. Fisher B.R., Eisler H.-J., Stott N.E., Bawendi M.G. *J. Phys. Chem., B* **2004**, *108*, 143-148.

95. Meloun M., Havel J., Högfeldt E. *Computation of Solution Equilibria.* Chichester: Ellis Horwood, **1988**.

96. Moerner W. E., Orrit M. *Science* **1999**, *283*, 1670-1676.

97. Nirmal M., Dabbousi B.O., Bawendi M.G., Macklin J.J., Trautman J.K., Harris T.D., Brus L.E. *Nature* **1996**, *383*, 802-804.

98. Cichos F., von Borczyskowski C., Orrit M. *Curr. Opin. Colloid Interface Scie.* **2007**, *12*, 272-284

99. Issac A., von Borczyskowski C., Cichos F. *Phys. Rev., B* **2005**, *71*, 161302 (R).

100. Kowerko D., Schuster J., von Borczyskowski C. *Mol. Phys.* **2009**, *107*, 1911-1921.

101. Schlegel G., Bohnenberger J., Potapova I., Mews A. *Phys. Rev. Lett.* **2002**, *88*, 137401(14).

102. Fisher B.R., Eisler H.-J., Stott N.E., Bawendi M.G. *J. Phys. Chem., B* **2004**, *108*, 143-148.

103. Zhang K., Chang H., Fu A., Alivisatos A.P., Yang H. *Nano Lett.* **2006**, *6*, 843-847.